J. Fluid Mech. (2001), *vol.* 432, *pp.* 91–125. Printed in the United Kingdom

Influence of jet exit conditions on the passive scalar field of an axisymmetric free jet

By J. MI, D. S. NOBES† AND G. J. NATHAN

Department of Mechanical Engineering, University of Adelaide, SA 5005, Australia

(Received 1 September 1999 and in revised form 28 September 2000)

The influence of initial flow conditions on the passive scalar field of a turbulent free jet issuing from the round nozzle is investigated in this paper by a review of the literature and a detailed experimental study. Two sets of distinctly different initial conditions are generated using two nozzle types: a smooth contraction and a long straight pipe. The present measurements of the passive scalar (temperature) field were conducted in a slightly heated air jet from each nozzle at a Reynolds number of 16 000 using identical experimental facilities and a single measurement technique. Significant differences between the flows from the two nozzles are revealed throughout the measured flow region which covers the axial range from 0 to 70 jet exit diameters. The study suggests that the differences observed in the statistics of the scalar field may be related to differences in the underlying turbulence structure of the jet in the near field. The present findings support the analytical result of George (1989) that the entire flow is influenced by the initial conditions, resulting in a variety of self-similar states in the far field.

1. Introduction

Turbulent jets have been studied both analytically and experimentally for many decades, not only because of their wide application but also because of their fundamental significance as a basic flow to the scientific research community. Previous studies relate predominantly to circular free jets, owing to their particular configuration of axisymmetry. In most cases, smoothly contracting nozzles have been used to produce a 'top-hat' velocity profile and to achieve a laminar flow state at the nozzle exit. This type of nozzle can minimize the pressure drop in the supply pipe and has a wide application in industry, e.g. burner nozzles and compact mixing devices. Nevertheless, numerous studies (e.g. Lockwood & Moneib 1980; Richards & Pitts 1993; Pitts 1991*a*, *b*) have also been performed using a long straight pipe to generate a jet. The pipe nozzle has the advantage of simplicity and thus has many practical applications, e.g. in burners, chimneys and stacks. A free jet from a long straight pipe emerges as a fully developed, turbulent pipe flow, which differs significantly from the initial conditions of a jet from a smooth contraction nozzle. The present paper explores the impact of this difference on the scalar statistical behaviour of an axisymmetric free jet.

We have chosen to measure the scalar field, rather than the velocity field, in the present study based on our observation from several previous studies (e.g. Browne, Antonia & Chambers 1984; Chua & Antonia 1986; So *et al.* 1990) that the former

† Current address: Optical Sensors Group, Department of Power Engineering and Propulsion, School of Mechanical Engineering, Cranfield University, Cranfield, Bedfordshire MK43 0AL, UK.

is more sensitive to differences in the underlying turbulence structure and thus to initial flow conditions. For example, Browne *et al.* (1984) showed in their figure 6 that there is quite a strong hump in the normalized centreline r.m.s. fluctuation of the temperature, and only a very weak hump in those of the three velocity components, in the developing region of a plane jet from a smoothly contracting nozzle. This observation is also supported by Sreenivasan (1996) who stated in his work on both velocity and scalar spectra that 'in inhomogeneous shear flows, the scalar field attains a semblance of universality only if the velocity field in its entirety is universal (not just one of its components)'.

The significance of initial conditions on the development of an axisymmetric jet mixing layer near the nozzle exit has been well documented in the literature (e.g. Bradshaw 1966; Flora & Goldschmidt 1969; Yule 1978; Husain & Hussain 1979; Hussain & Clark 1981; Zaman & Hussain 1984). However, less conclusive results are available regarding the initial-condition dependence of the jet flow farther downstream from the nozzle exit, especially in the fully developed far field. This is perhaps due to the classical belief that the influence of initial conditions of a flow decays rapidly with downstream distance and is eventually eliminated.

It is widely accepted (e.g. Chen & Rodi 1980; George 1989; Richards & Pitts 1993) that a jet issuing into quiescent surroundings continuously readjusts its dynamical behaviour relative to its initiated state, so that it asymptotically attains a self-similar (or self-preserving) state. According to the classical view, this asymptotic state depends only on the rate of momentum addition and is independent of other initial conditions (e.g. Townsend 1976). That is, the asymptotic growth rates of all jets are universal and the asymptotic normalized scalar fields of all jets are identical, regardless of jet initial conditions.

It has been well established through experimental studies that the scalar field of a turbulent jet achieves self-similarity in the region sufficiently far downstream from the nozzle (e.g. Dowling & Dimotakis 1990). There is, however, considerable confusion as to whether the asymptotic values that describe the scalar field are universal. Reviews on the subject (Chen & Rodi 1980; Gouldin *et al.* 1986; Pitts 1991*a*; Richards & Pitts 1993) report a wide range of different asymptotic values. For example, the reported spreading rate of a jet has a variation of $\pm 15\%$ (Richards & Pitts 1993), the reported centreline decay of the mean concentration has a variation of $\pm 10\%$ (Pitts 1991*a*) and the variation of the reported centreline r.m.s. fluctuation scaled with the local mean concentration exceeds $\pm 30\%$ (Pitts 1991*a*). In general, the cause of the variations has been attributed either to experimental error (e.g. Lockwood & Moneib 1980; Gouldin *et al.* 1986; Dowling & Dimotakis 1990) or to, perhaps subtle, differences in experimental conditions and apparatus (e.g. Gouldin *et al.* 1986; Dowling & Dimotakis 1990; Grinstein, Glauser & George 1995). Recently the validity of the classical hypothesis of universal similarity has been questioned (George 1989, 1995; Grinstein *et al.* 1995). The analytical work of George (1989) suggests that turbulent flows can asymptote to a variety of self-similar states determined by their initial conditions, in contrast to the classical treatments of Hinze (1975) and Chen & Rodi (1980).

The initial conditions of a jet are usually defined by the Reynolds number $Re_d = U_o d/\nu$ (where U_o is the exit bulk velocity, d is the nozzle exit diameter, and ν is the kinematic viscosity of fluid), the exit radial profiles of mean velocity and turbulence intensity, and the global density ratio of the jet fluid (ρ_e) to ambient fluid (ρ_∞), $R_\rho = \rho_e/\rho_\infty$. Pitts (1991*a*, *b*) investigated the effects of Re_d and R_ρ on the centreline scalar mixing behaviour of the axisymmetric turbulent jet issuing from a

long pipe. It is shown that differences in Re_d and R_ρ do not influence the far-field statistical behaviour of a jet. Richards & Pitts (1993) later extended the above investigation by varying both R_ρ and nozzle type (smooth contraction and pipe). They concluded that the asymptotic state of the scalar field of a jet, as characterized by the mean spreading rate, the centreline mean decay rate and the locally normalised r.m.s. fluctuation (sometimes referred to as 'unmixedness'), is not dependent on either the nozzle type or the density ratio R_ρ. These conclusions provide support for the classical hypothesis of universal self-similarity of the jet flow.

However, the conclusion reached by Richards & Pitts (1993) is somewhat at odds with the experimental findings of Dowling & Dimotakis (1990). The latter investigated the effect of Re_d on the self-similar behaviour of the concentration (scalar) field of a jet issuing from a smooth contraction nozzle. They observed a dependence on Re_d of both the far-field decay rate of the mean concentration field (their figure 7) and the shape of the radial distribution of the r.m.s. concentration fluctuation (their figure 11). Recently, Boersma, Brethouwer & Nieuwstadt (1998) have also questioned the classical hypothesis. These authors applied direct numerical simulation (DNS) to study the effect of different initial velocity profiles on the mean velocity and turbulence fields of an axisymmetric jet in the region $x/d \leqslant 42$ for $Re_d = 2400$. Although this study does not use a flow which extends far enough to reach truly self-similarity in the far field, it suggests that the asymptotic state of the flow may vary with different initial velocity profiles. The observations of Dowling & Dimotakis (1990) and Boersma *et al.* (1998) contradict the classical hypothesis of universal similarity and thus lend support to the analytical result of George (1989) that a variety of self-similar states are possible depending on the initial conditions. However, to our knowledge, no definitive study is available in the literature to resolve the issue of the impact of initial conditions on turbulent jet flows.

George (1989) conducted an analytical study with a view to provide a suitable framework for the possible relationship between self-similarity, initial conditions and large-scale coherent structures. He argued that the apparent discrepancies in measurements of various different flows presented above lie not in the experiments themselves nor in the concept of self-similarity, but rather in the restrictive manner in which the classical self-similarity analyses have been carried out. Using a more general similarity analysis, George showed that there exists a multiplicity of self-similar states (for a particular type of flow) and that each asymptotic state is uniquely determined by the initial flow conditions. Accordingly, the initial conditions of a turbulent flow, such as a jet or a wake flow, will affect the downstream development throughout the whole flow field.

The main objective of the present study is to verify the analytical result of George (1989) for an axisymmetric jet flow using an identical experimental technique, arrangement and measuring environment for two different initial conditions, and thus to clarify the above ambiguity. More specifically, the present paper seeks:

(i) to quantify, for the near field and transition region of an axisymmetric jet, the differences in statistical scalar properties which arise from the different initial conditions;

(ii) to determine whether or not there is a statistical difference in the far-field scalar properties of an axisymmetric jet as a result of different initial conditions.

To achieve the above objectives, we conduct both a literature review and an experimental investigation. The two sets of initial conditions which we have chosen are produced by a smooth contraction nozzle and a long straight pipe. Results from previous investigations of the scalar field are reported and reviewed in § 2,

by separating out those measurements performed with a smooth contraction nozzle from those performed with a pipe. The experimental investigation, which follows in §§ 3 to 6, uses a single measurement technique to quantify the jet scalar field and a planar flow visualization technique to image the flow structure of each jet. In § 4, initial conditions of the two jets are quantified while, in § 5, the differences in the flow structure within the near-field and transitional regions are explored. We present the scalar statistical properties in § 6, with some discussion, and provide further comments on the asymptotic state of the jet in § 7. Our conclusions are presented in § 8.

2. Review of previous studies of the scalar field of a jet

2.1. *Self-similarity concepts*

Self-similarity in the classical sense implies that the jet mixing field can be characterized using appropriately normalized parameters which depend on only one velocity (or a scalar quantity) and one length scale (e.g. Townsend 1976; Tennekes & Lumley 1972; Hinze 1976). Two dimensionless length scales commonly used to specify turbulent statistical properties are

$$\chi = \frac{x - x_o}{d_\varepsilon} \tag{1}$$

for the axial distance and

$$\eta = \frac{r}{x - x_o} \tag{2}$$

for the radial distance. Here, x denotes the axial distance downstream from the nozzle exit, x_o represents the x-coordinate of the jet's virtual origin, r is the radial distance from the jet centreline and d_ε is the effective diameter (sometimes referred to as 'momentum' diameter) of the nozzle. The effective diameter d_ε is defined as

$$d_\varepsilon = \frac{2M_e}{\sqrt{\pi \rho_\infty J_e}} \tag{3}$$

where

$$M_e = \int_0^{d/2} 2\pi \rho_e U_e r \mathrm{d}r$$

is the exit mass flux,

$$J_e = \int_0^{d/2} 2\pi \rho_e U_e^2 r \mathrm{d}r$$

is the exit momentum flux for the jet, ρ_e is the jet exit density, ρ_∞ is the density of the surrounding fluid, and U_e is the mean jet exit axial velocity. The concept of the effective diameter d_ε is used in the present discussion, following other researchers (Thring & Newby 1953; Beer, Chigier & Lee 1962; Becker *et al.* 1967; Dowling & Dimotakis 1990; Pitts 1991*a*, *b*; and Richards & Pitts 1993), to account for the effects of both the initial fluid density and mean velocity profile of the jet.

In cylindrical coordinates, the self-similar radial profiles of the scalar mean, Θ, and the scalar r.m.s., $\theta' = \overline{\theta^2}^{1/2}$, can be expressed, respectively, as

$$\Theta(x, r) = \Theta_c(x) f(\eta) \tag{4}$$

and

$$\theta'(x, r) = \Theta_c(x) g(\eta). \tag{5}$$

In (4) and (5), $\Theta_c(x)$ is the local maximum of $\Theta(x,r)$ which is found at the centreline $r=0$; the functions $f(\eta)$ and $g(\eta)$ are both smooth with $f(0)=1$. Along the jet centreline, $\Theta_c(x)$ varies with the reciprocal of the downstream distance from a virtual origin, which may be expressed as

$$\frac{\Theta_c}{\Theta_e} = K_1\left(\frac{d_\varepsilon}{x-x_{o1}}\right). \tag{6}$$

A virtual origin (x_{o1}) and a decay constant (K_1) are determined from experimental data presented in this form. The present notation for the virtual origin has been chosen to signify that this origin is derived from the variation of Θ_e/Θ_c which has a slope of $1/K_1$ in the far field, and to differentiate it from the virtual origin derived from the half-radius, a point discussed later in the paper.

The spreading of the jet scalar field is typically characterized by the scalar half-radius, $r_{1/2}$, defined as the radial location at which the local mean scalar is equal to half its value at the centreline, i.e. $\Theta(x,r_{1/2}) = 0.5\Theta_c(x)$. In the self-similar region, $r_{1/2}$ varies linearly with x so that

$$\frac{r_{1/2}}{d_\varepsilon} = K_2\left(\frac{x-x_{o2}}{d_\varepsilon}\right), \tag{7}$$

where K_2 is the spreading rate of $r_{1/2}$ and x_{o2} is the virtual origin associated with the half-radius $r_{1/2}$.

From (4) and (5), the normalization of the centreline r.m.s. scalar fluctuation $\theta'_c(x)$ by $\Theta_c(x)$ leads to

$$\frac{\theta'_c(x)}{\Theta_c(x)} = g(0), \tag{8}$$

which indicates that the ratio of $\theta'_c(x)$ and $\Theta_c(x)$ should be constant in the self-similar region.

2.2. *Previous measurements*

A review of previous experimental investigations of the scalar field of an axisymmetric turbulent free jet has been undertaken to assess the effect of initial conditions. Many of these investigations tested for self-similarity of the scalar field using scaling arguments similar to those relations presented in § 2.1. Typical results from those investigations obtained with a jet issuing from a smooth contraction are shown in table 1 and those of a jet from a pipe are presented in table 2. Listed are the first author, nozzle type, global density ratio (ρ_e/ρ_∞), co-flow to jet speed ratio (U_∞/U_e), Reynolds number (Re_d), the measurement range of x/d and the scalar measurement technique. The tables present the measured values of $K_1, K_2, x_{o1}/d, x_{o2}/d$ and θ^*_{asy} which is the asymptotic value of $\theta^*_c \equiv (\theta'/\Theta)_c$. The investigations have been selected to include only those in which the ambient fluid was either totally quiescent or introduced co-axially as a very low-speed stream and with density ratios in the range $0.5 < \rho_e/\rho_\infty < 1.5$. The selected ratio of free-stream velocity (U_∞) to jet exit velocity (U_e) was limited to less than 5% since a jet with $U_\infty/U_e \leqslant 5\%$ will develop to closely approximate a self-similar state (Nickels & Perry 1996), while those with higher U_∞/U_e never reach self-similarity (e.g. Antonia & Bilger 1973, 1976; Smith & Hughes 1977). All values of K_2 in tables 1 and 2 are based on the effective diameter, d_ε, of the initial jet, as defined in (3). In many cases, this has required applying a correction to the original data based on the actual diameter d or $d_{TN} = d(\rho_0/\rho_\infty)^{1/2}$, where d_{TN} is the Thring–Newby (1953) form. For the majority of previous investigations, the jet-exit velocity profile is not provided.

First author	ρ_e/ρ_∞	U_∞/U_o	Re_d	K_1	x_{o1}/d	K_2	x_{o2}/d	θ'_c/Θ_c	$x/d =$	Technique
Richards (1993)	1.552	0	25000	4.76	1.6 ± 3.9	0.113 (0.126)	3.6 (10.8)	0.230	30–50	Rayleigh scattering
Dowling (1990)	1.0	0.4%	5000	5.11	—	0.114	—	0.230	30–90	Rayleigh
	1.05		16000	4.73	—	0.114	—	0.237	20–80	scattering
Grandmaison (1982)	1.0	0	27000	5.43	1.67	0.105	1.67	—	2–40	Mie scattering
Becker (1967)	1.0	0	54000	5.59	2.4	0.106	2.4	0.22	0–32	Mie scattering
McQuaid (1974)	1.38	0	10000	4.52	−0.01	—	—	0.36	5–20	Hot wire
Ebrahimi (1977)	1.0	0	9500	5.78	—	—	—	—	0–80	Mie scattering
			15400	4.30	0		0	0.25	0–50	
			39600	4.40	—		—	—	0–100	
Chua (1986)	0.91	0	17700	4.63	−2.3	0.106	−1.4	0.19	0–40	Cold wire
So (1990)	0.64	0	4300	5.51	2.0	0.107	2.0	0.27	0–24.5	Laser/hot-wire
Present	0.85	0	16000	4.48	3.5	0.111	−1.0	0.24	0–64	Cold wire

TABLE 1. Previous scalar measurements for an axisymmetric jet from a smooth contraction nozzle.

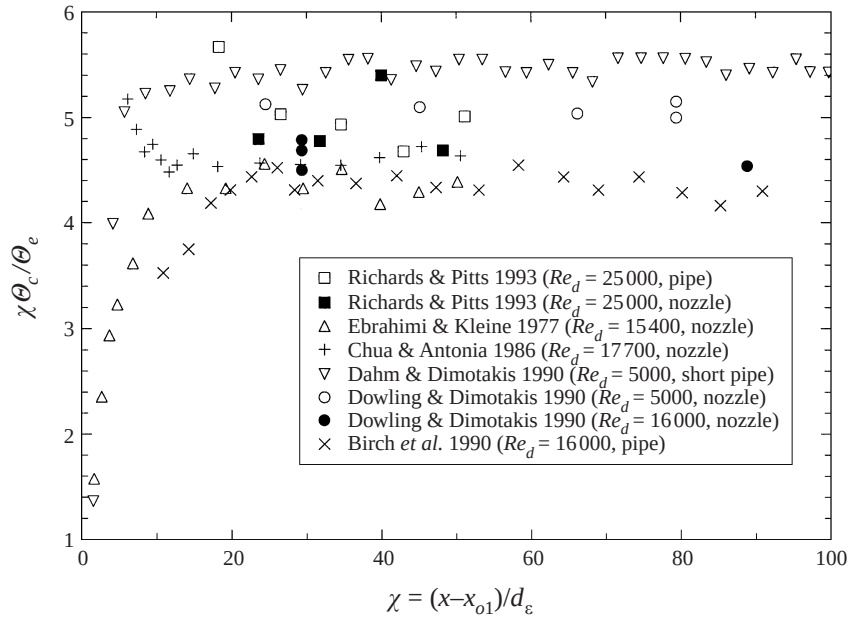

FIGURE 1. Comparison of previous measurements of $\chi\Theta_c/\Theta_e$ with reference to the nozzle type. Note that Dahm & Dimotakis (1990) used a short pipe (of $8d$ in length) following a smooth contraction.

We have made corrections using $d_\varepsilon = 0.97d_{TN}$ for the smooth contraction case and $d_\varepsilon = 0.99d_{TN}$ for the pipe case, where the factors 0.97 and 0.99 were obtained from the present exit-velocity measurements shown later in § 4.1. These values coincide with those estimated by Dowling (1988).

An examination of tables 1 and 2 shows the wide variability that exists in all parameters including the centreline mean decay rate (K_1) and the spreading rate of the scalar field (K_2). The centreline decay rate for the smooth contraction jet ($4.48 \leqslant K_1 \leqslant 5.59$) exhibits values over a range which overlaps that for the pipe jet ($4.42 \leqslant K_1 \leqslant 5.44$). Any influence of initial conditions is therefore not immediately apparent. An alternative method of viewing the centreline decay rate of a jet is to scale the normalized centreline scalar with the dimensionless axial position of the measurement. Figure 1 presents data in this form, $\chi\Theta_c/\Theta_e$ vs. χ, as adopted by Dahm & Dimotakis (1990) and contains data from some investigations cited in tables 1 and 2, some of which were not presented in this form in the original papers. Plotting the data in this manner graphically illustrates that most sets of data achieve self-similarity as indicated by an asymptotic approach to a horizontal straight line. However, in contrast to what is expected from the classical theory, there are a variety of asymptotic values.

There is better agreement and a more consistent trend in previous measurements of the spreading rate, K_2, of the scalar field of a jet than in the decay rate (K_1). The jet scalar field from a smooth contraction nozzle ($0.106 \leqslant K_2 \leqslant 0.114$) can be seen to spread faster than that from a pipe nozzle ($0.104 \leqslant K_2 \leqslant 0.106$). There is a discernible difference, of about 5%, between the average value of K_2 obtained for jets issuing from a smoothly contracting nozzle (≈ 0.110) and that from a pipe nozzle (≈ 0.105). The small variation in the data of K_2 across the range of techniques and experimental conditions implies that the estimate of K_2, resulting from the measurement of $r_{1/2}$, is less sensitive to experimental errors and less dependent on Reynolds number than

First author	ρ_e/ρ_∞	U_∞/U_o	Re_d	K_1	x_{o1}/d	K_2	x_{o2}/d	θ'_c/Θ_c	$x/d =$	Technique
Richards (1993)	1.552	0	25 000	4.81	2.1 ± 1	0.104 (0.116)	4.2 (10.5)	0.23	20–60	Rayleigh scattering
Dahm (1990)*	1.0	0	5000	5.41	—	—	—	0.225	0–300	LIF
Birch (1978)	0.56	0	16 000	4.44	5.8	0.097	0	0.27	0–70	Raman scattering
Lockwood (1980)	0.54	0	50 400	5.44	2.0	0.132	2.0	0.21	0–50	Thermo-couple
Pitts (1991)	1.02	4.3%	3960	4.42	−0.35	—	−0.35	0.23	2–31.5	Rayleigh scattering
Pitts (1984)	0.55	3.3%	4130	4.50	−1	0.104	0	0.23	0–30	Rayleigh scattering
Present	0.85	0	16 000	4.64	4.73	0.102	1.3	0.218	0–70	Cold-wire

TABLE 2. Previous scalar measurements for an axisymmetric jet from a long pipe. * The nozzle consists of a short pipe of length-to-diameter ratio of 8 that follows a smooth contraction. Therefore, the exit flow is not fully developed. In addition, their experiments were performed in water so that the Schmidt number is different by three orders of magnitude.

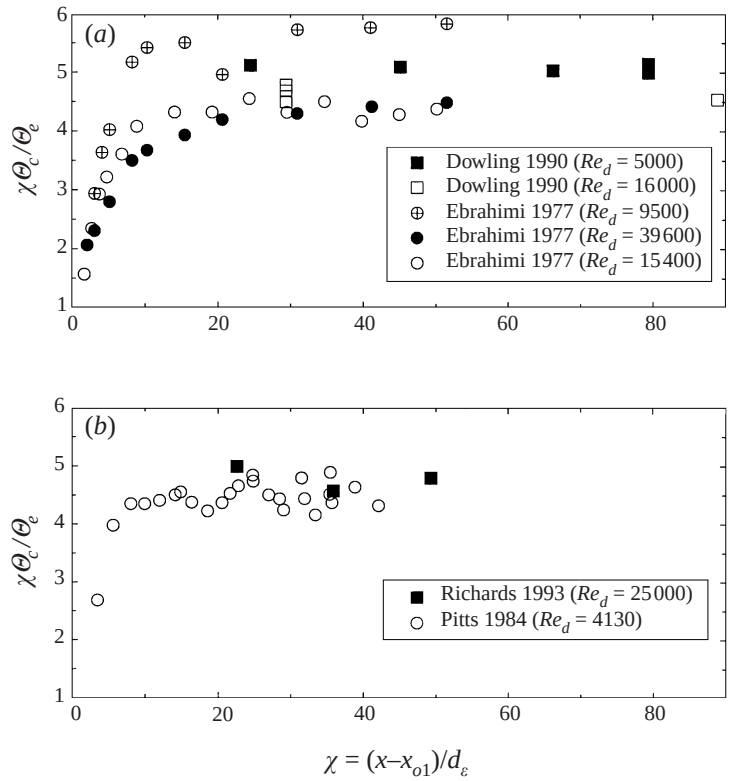

FIGURE 2. Comparison of previous measurements of $\chi\Theta_c/\Theta_e$ showing the effect of the Reynolds number for (*a*) a smooth contraction nozzle and (*b*) a pipe nozzle.

is that of K_1. This insensitivity can be explained as follows. The half-radius $r_{1/2}$ is defined as the radial location at which the scalar mean $\Theta(x,r)$ equals half its value on the centreline, i.e. $\Theta(x,r) = 0.5\Theta_c(x)$, so that $r_{1/2}$ is estimated in practice from the radial profiles of $\Theta(x,r)$. Since any systematic experimental error contaminates all measured $\Theta(x,r)$ equally, the estimate of $r_{1/2}$ is thus expected to be degraded less than the mean scalar Θ itself.

As indicated in the Introduction, Dowling & Dimotakis (1990) reported an influence of Reynolds number (Re_d) on the decay rate K_1: for $Re_d = 5000$, $K_1 \approx 4.73$ and for $Re_d = 16\,000$, $K_1 = 5.11$ in their investigation of a jet from a smooth contraction nozzle. The Re_d dependence is also evident in the data of Ebrahimi & Kleine (1977), which, together with the data of Dowling & Dimotakis (1990) are shown in figure 2(*a*). Note that both investigations varied the Reynolds number independently and were made using smooth contraction nozzles, although with different measurement techniques. The original data of Ebrahimi & Kleine (1977) were presented in the form Θ_c/Θ_e vs. x/d in their figure 4 ($Re_d = 9500$ and 39 600) and figure 9 ($Re_d = 15\,400$) and has been transposed for figure 2(*a*). Figure 2(*a*) demonstrates the dependence of $\chi\Theta_c/\Theta_e$ on Re_d in the data sets of both investigations. This dependence appears at first glance to contradict the finding of Pitts (1991*b*) who varied Re_d from 3950 to 11 880 and measured mean and r.m.s. fluctuation of jet-fluid mass fraction along the centreline of an axisymmetric jet and showed that the slope ($= 1/K_1$) of the linearized streamwise variation of Θ_e/Θ_c is nearly independent of Re_d and that the virtual origin for the data moves downstream with increasing Re_d. However, Pitts' investigation was

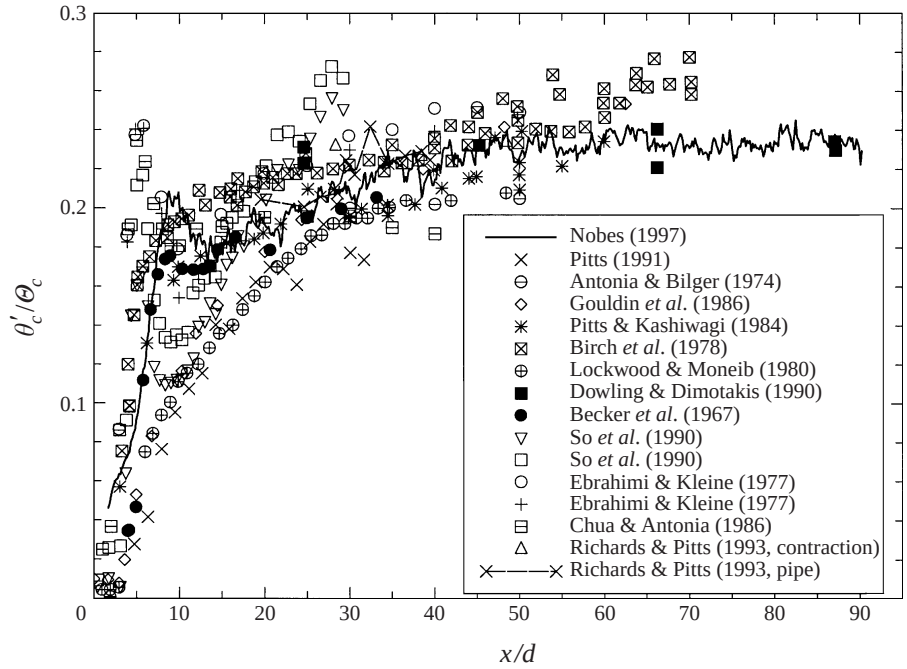

FIGURE 3. Centreline distributions of the normalized r.m.s. scalar fluctuation $\theta^* = \overline{\theta_c^2}^{1/2}/\Theta_c$, compiled from all previous investigations cited in tables 1 and 2.

made with the jet originating from a long pipe and issuing into a co-flowing air stream with the velocity ratio $5\% < U_\infty/U_e < 9\%$. The same conclusion of the independence of K_1 of Re_d for a pipe jet can also be drawn from other scalar measurements by Pitts and coworkers for a broader range of Re_d. Figure 2(*b*) compares the result of Richards & Pitts (1993) at $Re_d = 25\,000$ with that of Pitts & Kashiwagi (1984) at $Re_d = 4130$. Both used a methane jet originating from the same long pipe nozzle with a 6.35 mm ID. The results coincide with the previous finding of Pitts (1991*b*). It is thus logical to conclude that a Re_d dependence of K_1 exists for the jet from a smooth contraction nozzle, at least when $Re_d < Re_{cr}$ (a critical value), but is negligible for the jet from a long pipe. Further support for a Reynolds-number dependence for the smooth contraction nozzle is found in the mean velocity data reported recently by Malmström *et al.* (1997). Their figure 6 shows that the far-field, centreline mean velocity decay factor K, defined by $U_c/U_e = K[d/(x - x_o)]$, increases with Re_d when $Re_d < Re_{cr}$, and also that Re_{cr} varies significantly with the nozzle exit diameter (d).

The streamwise evolution of the normalized r.m.s. scalar fluctuation $\theta_c^* = (\theta'/\Theta)_c$ along the jet centreline, in the form θ_c^* vs. x/d, is shown in figure 3 for all of the studies cited in tables 1 and 2. It is evident that a range of values for θ_c^* has been determined from the different data sets throughout the flow field. Once again it is noted that, according to the classical hypothesis of universal similarity, θ_c^* should asymptote to the same value in the far field for all jets. The scatter is also evident in all previous publications that contain reviews, e.g. see Chen & Rodi (1980) and Gouldin *et al.* (1986). However, a closer investigation reveals that the streamwise development of θ_c^* differs depending on whether the jet is issuing from a smooth contraction nozzle or from a pipe nozzle, especially for $x/d < 15$. The differences are highlighted by

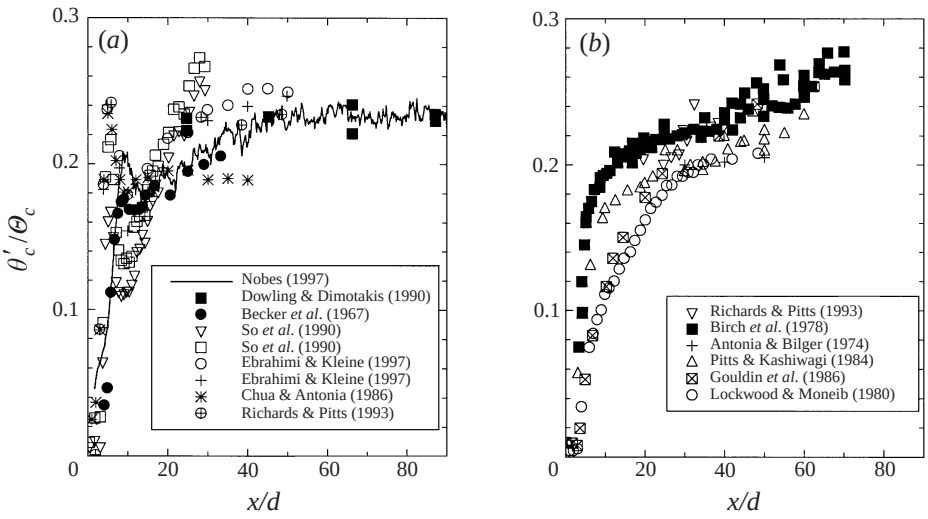

FIGURE 4. Centreline distributions of the normalized r.m.s. scalar fluctuation $\theta^* = \overline{\theta_c^2}^{1/2}/\Theta_c$ in the jets (*a*) from the smooth contraction nozzles and (*b*) from the pipe nozzles.

separating the data obtained with jets issuing from a smooth contraction, figure 4(*a*), from that obtained with jets issuing from a straight pipe, figure 4(*b*).

Figure 4(*a*) shows that for all jets issuing from a smooth contraction nozzle, a local maximum, or a hump, is present in the near field. There is no corresponding hump in the data for the pipe jets, figure 4(*b*). The presence of the hump has been attributed to experimental errors by some previous researchers (e.g. Lockwood & Monieb 1980) and, more specifically, to spatial resolution issues in the near field (e.g. Lockwood & Monieb 1980; Dowling & Dimotakis 1990). The data suggest, however, that the presence or absence of the hump is associated with the initial conditions and that there are genuine differences between the near-field flow issuing from a pipe nozzle and that from a smooth contraction nozzle. This difference will be discussed later in § 5.

Figures 3 and 4 also reveal a range of values for the far-field 'asymptotic' value of $\theta_c^* = \theta_{asy}^*$ measured by different researchers. Tables 1 and 2 present the values and show that θ_{asy}^* varies between 0.19 and 0.36. Since some of the previous investigations did not genuinely extend into the fully developed far field, or did not achieve an asymptotic value, we have reported θ_{asy}^* as the value of θ^* obtained at the maximum value of x/d for which measurements were obtained. A value of θ_{asy}^* between 0.21 and 0.23 has been generally accepted as that to be used for a general similarity solution of the scalar field (Chen & Rodi 1980; Pitts 1991*a*; Dowling & Dimotakis 1990). Values far from this are generally ignored in other reviews of the literature.

Experimental errors and spatial resolution issues are widely cited to be a major cause for the disparity in the measurement of θ_{asy}^*. The absolute error in θ_{asy}^* is the sum of those from θ_c' and Θ_c. However, the disparity is seldom attributed to the uncertainty between different experiments conducted by different researchers due to the wide range of experimental facilities and jet boundary or surrounding conditions. A variety of measurement techniques is evident in tables 1 and 2 and has been noted in a number of research and review papers (e.g. Gouldin *et al.* 1986; Dowling & Dimotakis 1990). However, such a wide scatter, $\pm 30\%$, appears too large to be attributed solely to measurement errors or differences in the techniques. The effect of jet surrounding

conditions should not be omitted. In fact, it is argued fairly convincingly by George (1990) and Hussein, Capp & George (1994) that surrounding conditions are important to the far-field jet development. Hussein *et al.* (1994) indicated that the confinement of a jet in a relatively small enclosure can reduce the jet momentum through loss to the external return flow, thus accelerating the decay of jet mean velocity even in the self-similar region. We also note that prior to the work of Richards & Pitts (1993), several previous investigators have cited the influence of initial conditions as a potential source of variation between previous results (Lockwood & Moneib 1980; Gouldin *et al.* 1986; Dowling & Dimotakis 1990). Unfortunately, it is not possible to separate the effect of the exit conditions from the effects of experimental errors and those associated with inevitable differences in the surrounding environment, since few previous papers reported full experimental details and measurement uncertainties. In this context, we have designed two experiments to conduct passive scalar (temperature) measurements using identical experimental set-up and surrounding environment, but with significantly different jet exit conditions produced by a smooth contraction nozzle and a long pipe. This minimizes the experimental uncertainty.

2.3. *Summary of previous investigations*

The key findings from the review of previous investigations of the scalar field of an axisymmetric free jet can be summarized as follows:

(i) There is strong evidence that the scalar decay rate in the self-similar far field depends on the initial Reynolds number when the jet issues from a smooth contraction. However, the Reynolds number dependence for jets originating from a long pipe is much weaker and may be negligible;

(ii) There is evidence that the spreading rate of the scalar field is larger for a jet issuing from a smooth contraction nozzle than from a long pipe;

(iii) There are clear differences between the near-field behaviour of a jet issuing from a pipe and that issuing from a smooth contraction for the locally normalized r.m.s. scalar fluctuations on the centreline. There is a distinct hump immediately downstream from the potential core for a jet issuing from a smooth contraction nozzle, while no hump exists for the jet issuing from a long pipe.

3. Experimental details

3.1. *Temperature and velocity measurements*

In the present experiments, the scalar field of the jet flow was marked by a passive temperature differential, with the air in the jet slightly heated relative to the surrounding ambient air. Two different nozzles, i.e. a smooth contraction nozzle and a long straight pipe, were employed in the experiments. The smooth contraction has a profile described by the relation $R = 40 - 30\sin^{1.5}(90 - 9x'/8)$, contracting from a diameter of 80 mm to the exit diameter (d) of 14 mm (figure 5*a*). The long straight round pipe has a length of 72 inner diameters ($d = 10$ mm; see figure 5*b*).

The jet facility consists of a vertical, cylindrical plenum chamber with an internal diameter of 80 mm and a length of 900 mm. It is attached to an in-line diffuser and an electrical heater (figure 6). Filtered and compressed air, with a maximum pressure of 500 kPa at 20 °C, was supplied through the heater and the plenum to the nozzle. The bulk exit velocity of the jet, U_o, was controlled by varying the plenum pressure and measured by an orifice-type flow rate meter (and checked by a standard Pitot tube), while the exit temperature was controlled by adjusting the heater power rate. The jet facility and nozzles were insulated to achieve a uniform mean temperature profile at

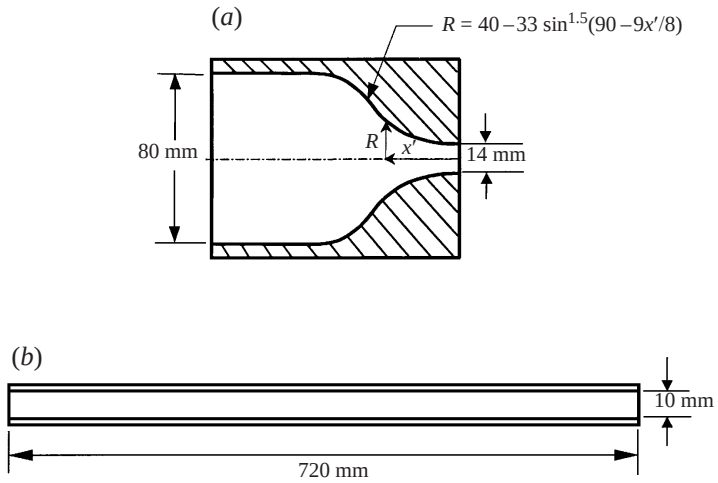

FIGURE 5. Schematic diagrams of (*a*) the smooth contraction nozzle and (*b*) the long straight pipe nozzle, used in the present experiment.

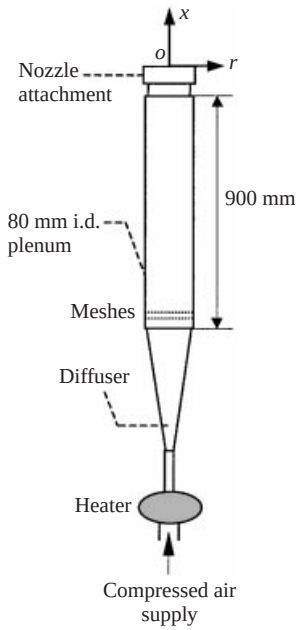

FIGURE 6. Schematic of the jet facility.

the exit. For both cases, the Reynolds number $Re_d(\equiv U_o d/\nu)$ is about 16 000; the exit mean temperature Θ_e is around 50 K above ambient. Throughout the paper, the term 'temperature' denotes the 'temperature above ambient' ($\Theta_a \simeq 288$ K). Note that the same value of Re_d also implies the use of nearly identical rates of initial momentum addition for the two jets (see the Appendix). It is also important to note that Grashof number $Gr_d \equiv g d^3(\Theta_e + 273)\nu^{-2}\Theta_a^{-1}$ is estimated to be 12 440 so that the ratio Gr_d/Re_d^2 is extremely small ($= 2 \times 10^{-5}$). This small ratio implies that the effect of buoyancy is negligible and thus that temperature acts only as a passive contaminant. During the course of experiments, care was taken to minimize laboratory draughts.

The present temperature measurements were conducted in the region $0 < x/d \leqslant 70$ in the $(x;r)$ central plane ($r = 0$). The measuring probe consists of a short length of Wollaston wire (Pt–10% Ph) operated with an in-house constant-current (0.1 mA) circuit, which is usually termed a 'cold-wire' probe. Most of the instantaneous temperature signals $\tilde{\Theta} = \Theta + \theta$ were collected using a wire of 0.63 μm in diameter and about 0.6 mm in length. In the near-field high-velocity region, $x/d \leqslant 5$, the 0.63 μm wire frequently failed. Consequently these measurements were performed using a thicker wire with a diameter of 1.23 μm. The present measurements of jet velocities very near to the exit plane of each nozzle were carried out using a single hot-wire (5 μm tungsten) probe with an overheat ratio of 1.5, also at $Re_d = 16\,000$. The voltage signals for both temperature and velocity were offset and amplified through the circuits and then digitized by a personal computer with a 12-bit A/D converter. The signals were filtered at a cutoff frequency $f = f_c$ (typically 2.8 kHz) chosen to eliminate high-frequency noise and a sampling frequency of $2f_c$ was employed. The record duration was 20–30 s, in which typically 110 000 to 310 000 (instantaneous) data points were collected.

Experimental errors for various measured quantities are estimated to be: mean temperature $[\Theta] \approx \pm 1.5\%$; r.m.s. temperature $[\overline{\theta^2}^{1/2}] \approx \pm 2.0\%$; mean velocity $[U] \approx \pm 1\%$; r.m.s. velocity $[\overline{u^2}^{1/2}] \approx \pm 1.2\%$. These estimates were inferred from estimated inaccuracies in the calibration data and from the observed scatter in the measurements.

3.2. *Flow visualization*

Flow visualization was carried out using the method described by Nobes (1997). Air, seeded with oil droplets of approximately 0.6 μm diameter, was introduced at ambient temperature into each of the nozzles described above. Laser pulses of less than 4 ns at a wavelength of 532 nm from an Nd : YAG laser were expanded to form a thin (< 0.25 mm) light sheet using a cylindrical lens. The light scattered from the seeded particles was captured by a slow-scan, cooled CCD camera which has a two-dimensional array of 576×384 pixels. The camera was oriented perpendicular to the plane of the sheet. The collected images were transferred to the control computer via a GPIB interface, which was also used for communication with, and control of, the detector. A target image was used to provide accurate scaling of the flow.

4. Jet exit conditions

4.1. *Velocity*

The exit velocity profiles were obtained at $x/d = 0.05$ in each unheated air jet from the contraction nozzle and the pipe. Figures 7 and 8 present radial profiles of the axial velocity mean (U) and r.m.s. ($u' = \overline{u^2}^{1/2}$) for the two cases. In the figures, U_c is the centreline mean velocity, $\delta_m \equiv \int_0^{d/2} (U/U_c)(1 - U/U_c)\,\mathrm{d}y$ is the momentum thickness of the initial boundary layer from the smooth contraction. Distinct differences are evident in the profiles of both $U(r)/U_c$ and $u'(r)/U(r)$ for the two cases. While $U(r)$ exhibits a quasi-'top-hat' shape for the contraction case, it takes an '∩' shape for the pipe case. For the contraction case, the radial profile of U/U_c near to the nozzle wall approximates the Blasius relation (see the inset of figure 7), suggesting the initial boundary layer to be laminar (Schlichting 1968). For the pipe jet, the radial profile of U/U_c is fairly well described by the empirical power-law profile $(1 - 2r/d)^{1/n}$ with $n = 6.5$, confirming that the flow upstream from the pipe exit is fully developed pipe flow (e.g. Munson, Young & Okiishi 1998).

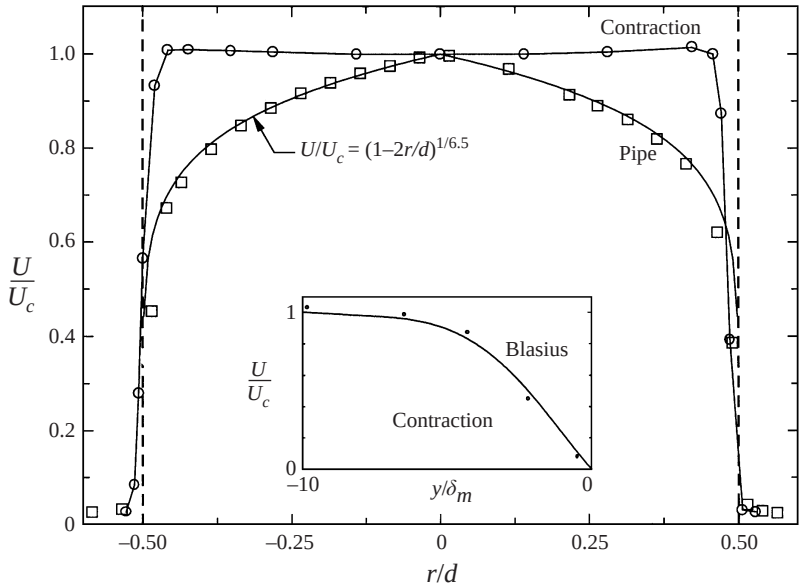

FIGURE 7. Radial profiles of the axial mean velocity (U) measured at $x/d = 0.05$ in the jets from the smooth contraction and pipe nozzles.

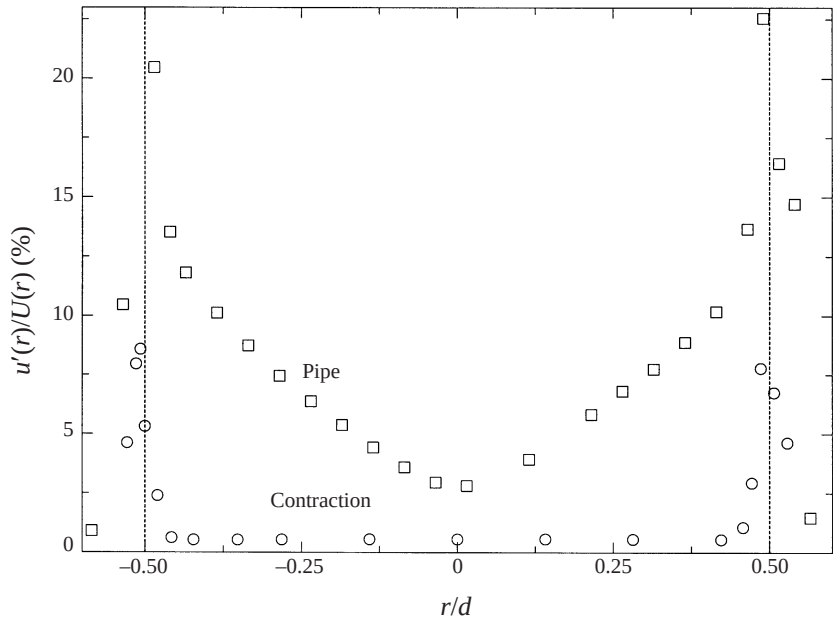

FIGURE 8. Radial profiles of the axial velocity r.m.s. (u') measured at $x/d = 0.05$ in the jets from the smooth contraction and pipe nozzles.

The initial boundary layer may be characterized by the boundary-layer displacement thickness defined as $\delta_d \equiv \int_0^{d/2}(1 - U/U_c)\mathrm{d}y$ and momentum thickness δ_m, although, strictly, it is not appropriate to use the term 'layer' to describe fully developed pipe flow. The values of δ_d and δ_m are very different for the two cases: $\delta_d = 0.004d$, $\delta_m = 0.0018d$ for the smooth contraction and $\delta_d = 0.063d$, $\delta_m = 0.047d$ for the pipe.

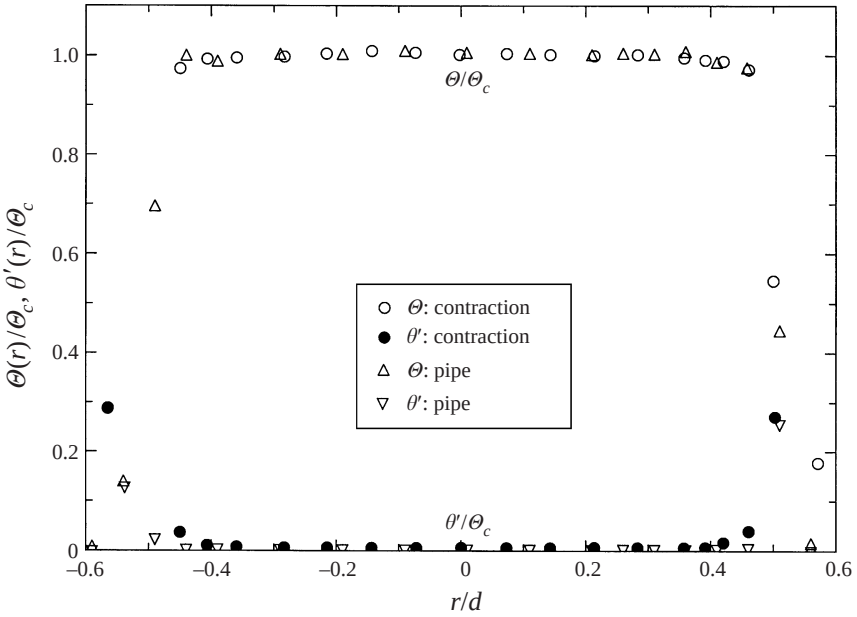

FIGURE 9. Radial profiles of the temperature mean (Θ) and r.m.s. (θ') measured at $x/d = 0.1$ in the jets from the smooth contraction and pipe nozzles.

Moreover, the relative initial turbulence intensity $u'(r)/U(r)$ is about 0.5% in the central region $r/d \leqslant 0.45$ of the exit plane for the contraction case. By contrast, it varies significantly between 3% (centre, $r = 0$) and 24% (around the pipe edge, $r = d/2$) across the pipe exit, which is similar to the data reported in the literature (e.g. Papadopoulos & Pitts 1998).

4.2. *Temperature*

Figure 9 presents the mean and r.m.s. profiles of the temperature, i.e. $\Theta(r)/\Theta_c$ and $\theta'(r)/\Theta_c$, obtained at $x/d = 0.1$ for both jets. Unlike the situation for the velocity, the exit temperature profiles of the two jets are nearly identical. They are generally uniform in a broad central region of the exit plane; more specifically, $\Theta(r)/\Theta_c \approx 1$ and $\theta'(r)/\Theta(r) \approx 0.52\%$ (contraction) and $\theta'(r)/\Theta(r) \approx 0.35\%$ (pipe) over the range $r/d \leqslant 0.4$. The high uniformity and low r.m.s. value in the passive temperature at the nozzle exit indicate that the differences in the velocity mean and r.m.s. define the differences in the initial conditions between the two jets for the present study.

5. The structure of near-field turbulence

The influence of the exit conditions on the near-field structure of a jet ($x/d < 8$) is demonstrated in the instantaneous planar images of the scalar field presented in figure 10. Figure 10(*a*) shows an image of the near field of the jet issuing from the smooth contraction nozzle and figure 10(*b*) shows that from the long pipe. The images are scaled to provide the same dimensionless field of the jet to facilitate a comparison. They have been selected from several hundreds of such images as being representative of the flows.

The structure of the near-field turbulence is distinctly different for the two jets, with large-scale ring-like vortices evident in the near field of the jet from the smooth

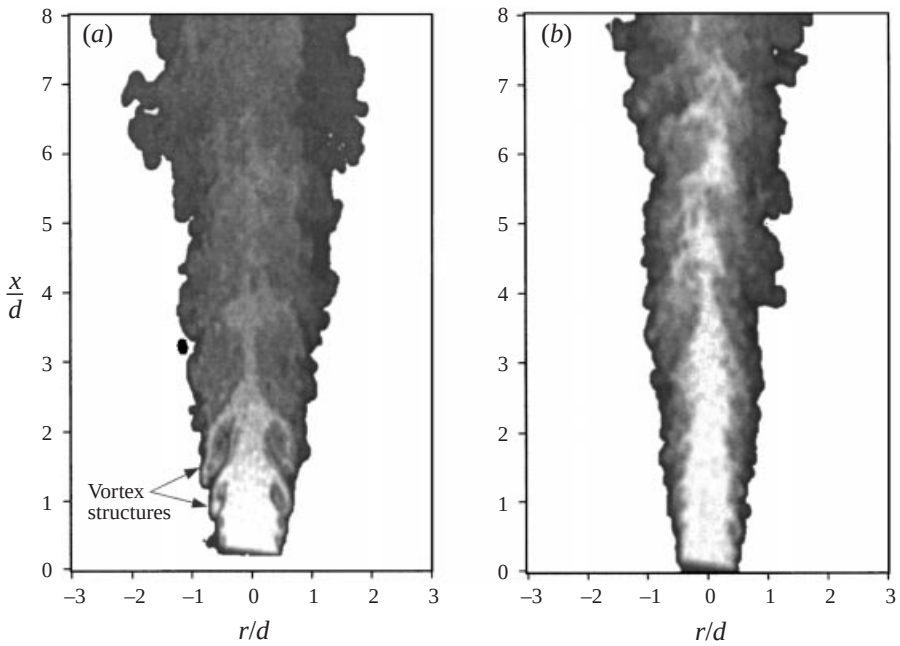

FIGURE 10. Mie scattering sideview of the two jets in the near field: (*a*) smooth contraction, (*b*) pipe.

contraction. The vortex structures are a direct result of the roll-up of the laminar boundary from the inner wall of the nozzle. These axisymmetric, toroidal vortices engulf both ambient and 'pure jet' fluid and 'pinch-off' the tip of the potential core of the jet at approximately $x/d = 3$. The toroidal structures propagate downstream and are evident throughout the series of image.

The formation of the primary vortices in a jet from a smooth contraction is known to originate from an instability within the shear layer (e.g. Ho & Nosseir 1981; Grinstein *et al.* 1995). A selective spatial amplification process of the naturally occurring, narrow-band disturbances leads to the regular formation of the primary ring-like vortices (Grinstein *et al.* 1995). When the initially laminar shear layer from a smooth contraction nozzle becomes unstable, velocity fluctuations increase in amplitude resulting in the roll-up of the shear layer into a train of azimuthal vortex elements. Any slight asymmetry in the spacing between two adjacent vortices, or inequality in their strengths, induces them to roll around each other, i.e. to pair, eventually forming a single larger vortical structure. In this pairing process, some non-vortical ambient fluid is trapped between the pairing vortices and mixed subsequently by the turbulent process (Winant & Brown 1974; Brown & Roshko 1974; Grinstein *et al.* 1995).

By contrast, small-scale turbulent structures dominate the near field of the emerging jet from the long pipe, which has a much thicker initial 'boundary layer'. Consequently, the core region of pure jet fluid is longer and does not begin to break down clearly until $x/d = 5$ (figure 10*b*). The flow within the pipe is fully turbulent and has significantly higher turbulence intensity than the flow from the smooth contraction. Various scales of turbulence are present at the pipe exit and provide initial disturbances of sufficient amplitude over a wide range of wavenumbers, overwhelming the natural narrow-band disturbances and therefore disrupting/suppressing the vortex formation process in the jet near field. As a result, few large-scale coherent vortical structures are

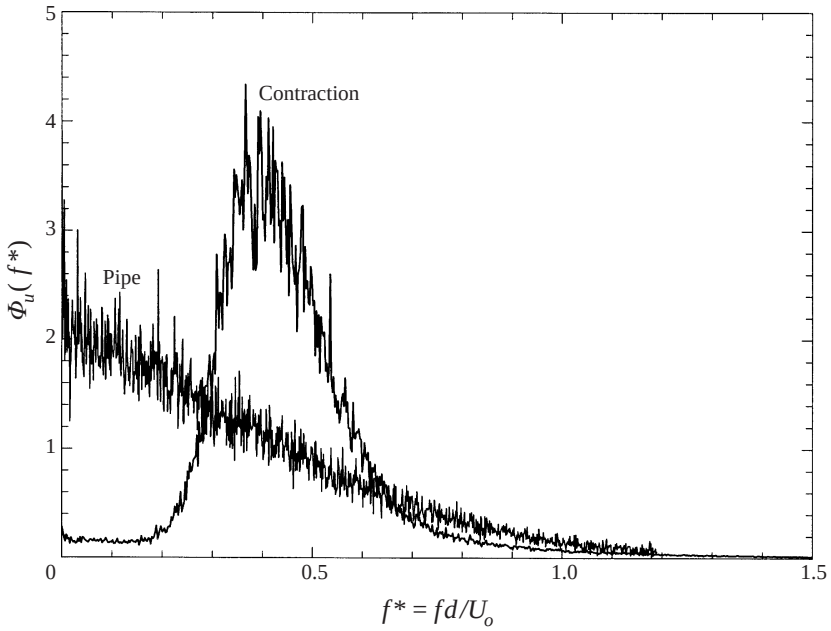

FIGURE 11. The velocity spectra obtained at $x/d = 3$ in the shear-layer in the two jets.

formed in the near field. Russ & Strykowski (1993) showed that the wavelength of the initial instability in the shear layer of a jet from a smooth contraction increases proportionally with the boundary-layer thickness. While it is not possible to directly extrapolate from a smooth contraction to a pipe, it can be expected that the formation of large-scale structures in the pipe jet will occur much farther downstream than that in the present jet from the smooth contraction. Some evidence of large-scale motion in the region $x/d \geqslant 6$ to 8 may be found in figure 10(*b*).

It is important to note that there are clear differences in the 'potential core' of the two jets. For the smooth contraction, the concentration/temperature scalar and velocity profile is uniform across the exit plane and there is a strong gradient in both profiles in the shear layer at the edge of the jet. This results in spatial coincidence of the maximum gradients of the mean velocity and mean scalar. In contrast, for the pipe case there is a uniform profile for the mean scalar field and a radially varying profile for the mean velocity field. Hence, the mean scalar and velocity profiles do not exhibit a similar form. The term 'potential core' is therefore used with quotation marks for the case of the pipe jet.

Quantitative aspects of the structure of the near-field turbulence can be gained from frequency spectra of the velocity fluctuations. The velocity spectrum $\Phi_u(f)$ was measured using a single hot wire in the unheated jets under the same conditions as described in § 4.1. Figure 11 presents $\Phi_u^*(f^*)$ against $f^* \equiv fd/U_e$, where $\int \Phi_u^*(f^*)\mathrm{d}f^* = 1$, obtained within the shear layer at $x/d = 3$ for both jets. A broad peak centred at $f^* = 0.40$ occurs in Φ_u for the jet from the smooth contraction. This value falls within the range (0.3–0.6) of the Strouhal number $St(\equiv f_1 d/U_e$, where f_1 denotes the frequency of formation of the vortex structures) measured by a number of previous investigators (e.g. Crow & Champagne 1971) and analysed by Ho & Nosseir (1981) for the jet from a smooth contraction nozzle. The exact magnitude of the dominant frequency depends on the state of the boundary layer at the nozzle exit and the

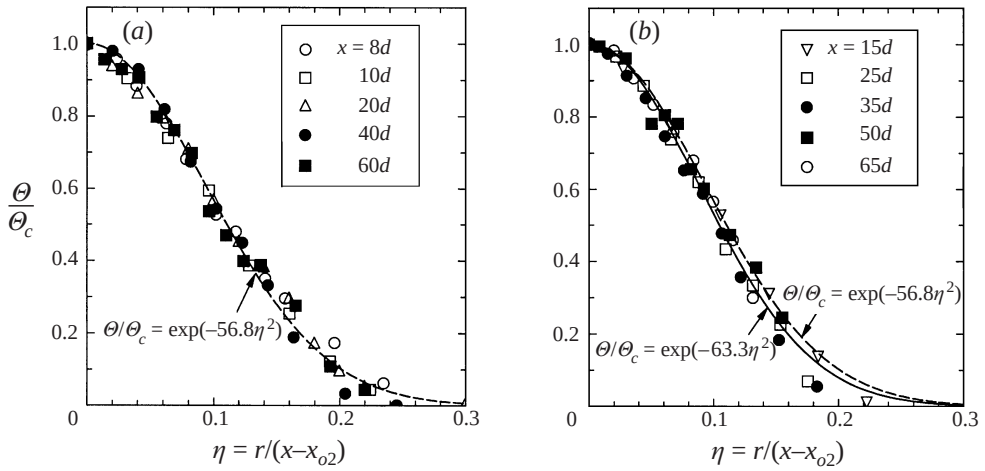

FIGURE 12. Radial profiles of the normalized temperature mean, $\Theta(x,r)$, at several values of x/d indicated on the plots in the jets from (*a*) the smooth contraction nozzle and (*b*) the pipe.

downstream distance (x). Thus, some different values of St are expected between nozzles that have different geometric shapes. The power spectral density $\Phi_u(f)$ for the pipe nozzle is very different and does not show a broad peak, indicating no preferred frequencies, and hence no dominant coherent structures in the flow. This is consistent with the images presented in figure 10.

6. The influence of jet exit conditions on the passive scalar field

6.1. *Mean scalar field*

Figures 12(*a*) and 12(*b*) show radial profiles of the mean temperature, $\Theta(x,r)$, for both the jet from the smooth contraction nozzle and that from the pipe at different axial stations through the developing region and the far field. The data are presented in the form $\Theta(x,r)/\Theta_c(x)$ vs. $\eta = r/(x - x_{o2})$, following equation (1). The location of the virtual origin, x_{o2}, has been obtained from the streamwise variation of the half-radius presented later in figure 15. Here, $x_{o2}/d = -1$ for the contraction case and $x_{o2}/d = 1.3$ for the pipe case. It is evident that the normalized radial profile for both jets is independent of x for the range $x/d > 10$. That is, the similarity equation (5) is satisfied, i.e. $\Theta(x,\eta) = \Theta_c(x)f(\eta)$. This indicates that self-similarity of the mean scalar field is established in the developing or transition region. As also demonstrated in the figures, the mean scalar field for both jets is described well by the Gaussian function

$$f(\eta) \equiv \frac{\Theta(x,\eta)}{\Theta_c(x)} = \exp(-A\eta^2), \tag{9}$$

where A is determined from a least-squares fit of the experimental data. The data show differences in the radial profiles of the two jets. The constant A is found to be 56.8 for the contraction case compared with 63.3 for the pipe. This compares to a value of 59 determined by Richards & Pitts (1993) for both jets. Figure 12(*b*) presents the fitted profile for both jets, namely the profile from figure 12(*a*) is transcribed to figure 12(*b*), to facilitate comparison. The broader profile of the jet from the smooth contraction nozzle indicates that this jet spreads at a faster rate than that from the pipe.

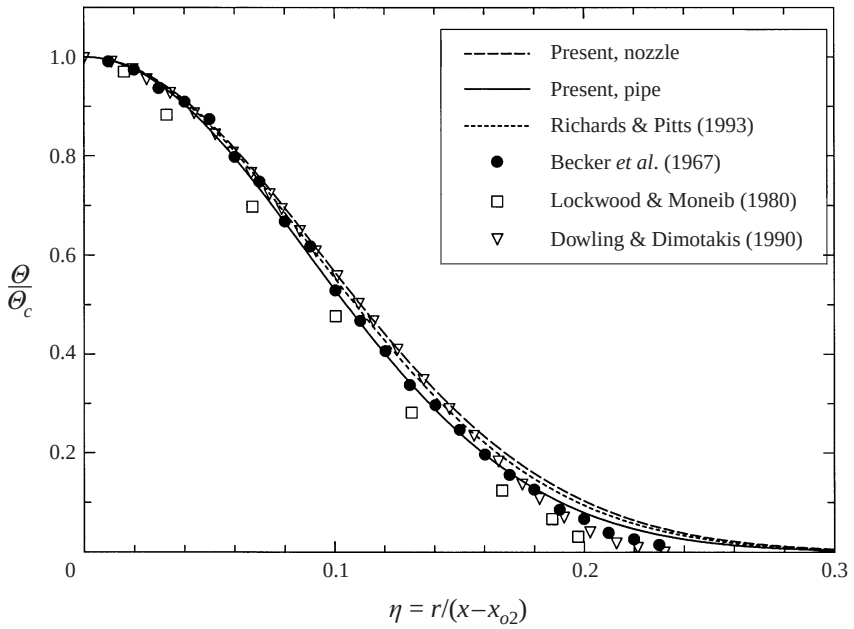

FIGURE 13. Comparison of the present result with those of previous experiments for the radial profiles of the normalized scalar mean $\Theta(x,r)$.

Note that the data presented in figure 12 have a different form of normalization from that commonly adopted in the literature (e.g. Becker, Hottel & Williams 1967; Birch *et al.* 1978; Lockwood & Moneib 1980; Chua & Antonia 1986). The abscissa has been normalized by the axial distance rather than the half-radius $r_{1/2}$ which gives $\eta = r/r_{1/2}$. Normalization by the half-radius (not presented) makes it difficult to detect any difference in $\Theta(x,r)/\Theta_c(x)$. This is partly because the ratio is forced to be 0.5 at $r/r_{1/2} \simeq 1$ for both cases. It is also clear that the use of $\eta = r/r_{1/2}$ absorbs the effects of initial conditions in $\Theta(x,r)/\Theta_c(x)$, exactly as deduced by George (1989, 1995) for the velocity field (see also Hussein *et al.* 1994). Figure 13 compares the present fitted Gaussian profiles of $f(\eta) = \Theta(x,r)/\Theta_c(x)$ with data previously published by Becker *et al.* (1967), Lockwood & Moneib (1980), Dowling & Dimotakis (1990) and Richards & Pitts (1993) (see tables 1 and 2 for more information on those studies). While some disparity is seen in the data sets, they nevertheless suggest that the scalar field of a jet issuing from a long pipe (Lockwood & Moneib 1980) does not spread as rapidly as that from a smooth contraction (Becker *et al.* 1967; Dowling & Dimotakis 1990).

The axial decay of the mean temperature along the centreline, $\Theta_c(x)$, is shown for both jets in figures 14(*a*) and 14(*b*). Figure 14(*a*) presents the data in the form Θ_c/Θ_e vs. x/d_ε and figure 14(*b*) in the form $\chi\Theta_c/\Theta_e$ vs. $\chi \equiv (x - x_{o1})/d_\varepsilon$. Here, Θ_e is the mean temperature above ambient at the jet exit and d_ε is the equivalent diameter of the nozzle as defined in equation (4). It is shown that, beyond $x/d_\varepsilon = 20$, Θ_c/Θ_e varies reciprocally with x for both jets and can be described by equation (6). However, K_1 and x_{o1} are not identical in the two cases: $(K_1, x_{o1}) = (4.46, 3.5d)$ for the smooth contraction and $(4.63, 4.7d)$ for the pipe. The decay rate of Θ_c is approximately 4% higher in the former case, as indicated by a smaller value of K_1.

Figure 15 compares the spreading rates of the two jets from the streamwise variations of the temperature half-radius $r_{1/2}$ at which $\Theta = 0.5\Theta_c$. Note that $r_{1/2}$ was

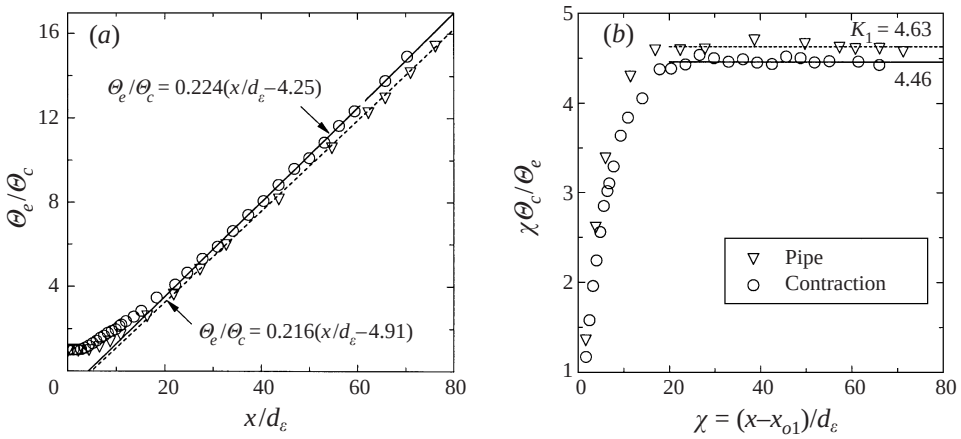

FIGURE 14. Streamwise variations of the normalized temperature mean, Θ_c, along the centreline of each jet. (*a*) Θ_c/Θ_e; (*b*) $\chi\Theta_c/\Theta_e$.

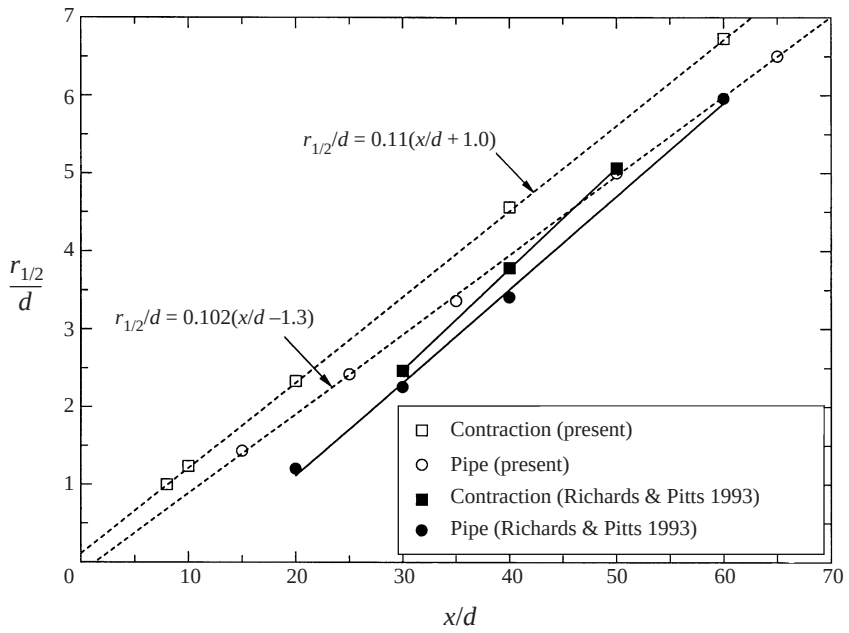

FIGURE 15. Streamwise variations of the scalar half-radius, $r_{1/2}(x)$, in the two jets.

determined from the radial profiles reported in figure 12. In both jets, $r_{1/2}$ varies linearly with x over the measured region and can be depicted using (7) as

$$\text{Contraction}: \quad r_{1/2}/d = 0.110(x/d + 1.0);$$

$$\text{Pipe}: \quad r_{1/2}/d = 0.102(x/d - 1.3).$$

The spreading rate (K_2) of the temperature field in the jet from the contraction is 7.5% higher than that from the pipe. The higher value of K_2 is logically consistent with the larger decay rate ($1/K_1$), figure 14, for the contraction case. The present observation agrees well with data obtained from previous studies reviewed in § 2.2. We have reproduced in figure 15 the data of Richards & Pitts (1993) for propane

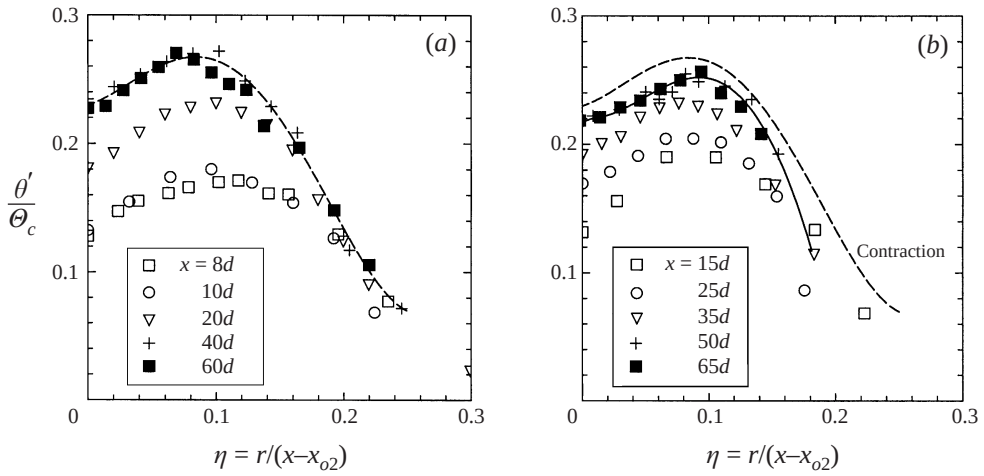

FIGURE 16. Radial profiles of the normalized temperature r.m.s. $\theta'_c(x,r)/\Theta_c(x)$ for the two jets at several downstream locations indicated on the plots: (*a*) smooth contraction; (*b*) pipe.

jets from a smooth contraction nozzle and a pipe both at $Re_d = 25\,000$. Both sets of experimental results demonstrate that the spreading rate of the jet from the smooth contraction is higher than that from the pipe. This contrasts with the deduction of Richards & Pitts (1993) that the slope of the linearized variation of $r_{1/2}(x)$ is nearly identical for the two jets. Note that their observation was obtained by discarding the first data point for the pipe case, as indicated in their text. Of interest also is that their mass-fraction scalar field appears to have a higher spreading angle than our temperature scalar field.

Some comments are made here on differences between the values of the virtual origin determined from $\Theta_c(x)$ and those determined from $r_{1/2}(x)$, i.e. x_{o1} and x_{o2}, both in the contraction jet and in the pipe jet. From figures 14 and 15, it can be estimated that $x_{o1} = 3.5d$ and $x_{o2} = -1.0d$ for the contraction case and that $x_{o1} = 4.7d$ and $x_{o2} = 1.3d$ for the pipe case. In both cases, the virtual origin of the centreline mean decay is farther downstream from the nozzle exit than that for the scalar half-radius. This observation contradicts the traditional assumption that x_{o1} and x_{o2} are equal (e.g. Hinze 1975 and Chen & Rodi 1980). However, it is consistent with the observation of Richards & Pitts (1993) that x_{o1} and x_{o2} are not equivalent in variable-density flows.

6.2. *Turbulent scalar fluctuation field*

Figures 16(*a*) and 16(*b*) present radial profiles of the normalised r.m.s. temperature fluctuations $\theta'(x,r)/\Theta_c(x)$, where $\theta' = \overline{\theta^2}^{1/2}$, for the two jets at five downstream locations within the transitional and far-field regions, as indicated in the figure legend. Relative to the mean temperature field, the r.m.s. temperature field develops to the self-similar state further downstream from the nozzle exit. The self-similar state of the r.m.s. scalar field is reached at $x \geqslant 40d$ for the smooth contraction case and $x \geqslant 50d$ for the pipe case, which is also seen in figure 17. As demonstrated in the figures, the r.m.s. temperature field evolves differently in both the streamwise and radial directions for the two jets. In the self-similar region, the r.m.s. level is clearly higher for the contraction case than for the pipe (figure 16*b*). This difference may be associated with more large-scale coherent structures in the jet from the smooth contraction, an issue discussed later in more detail in § 7.

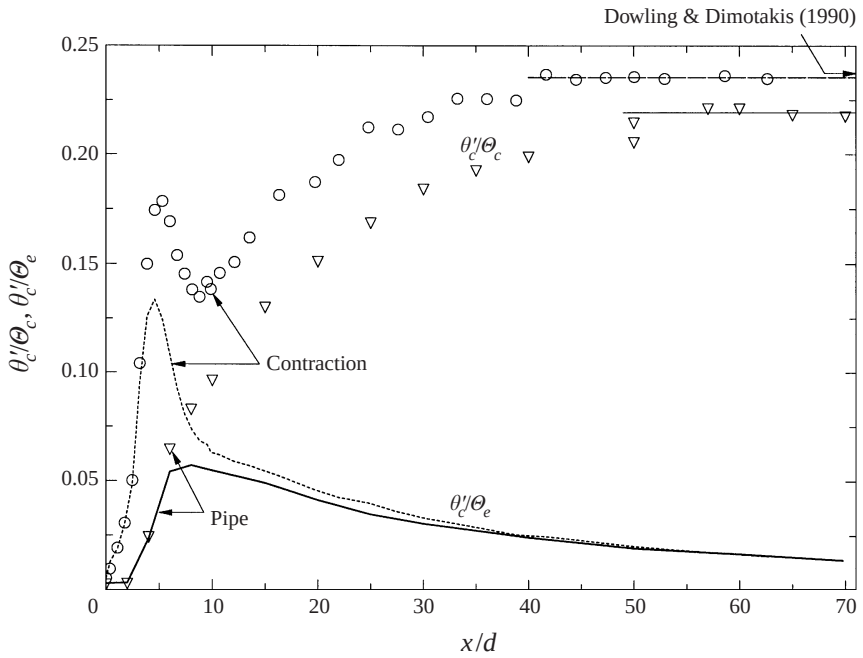

FIGURE 17. Streamwise variation of the temperature r.m.s. θ_c' along the jet centreline, for two different normalizations.

Figure 17 compares the streamwise development of the centreline r.m.s. temperature fluctuations (θ_c') for the two jets. Two normalization procedures are shown. The normalization of θ_c' by the exit mean temperature (Θ_e) gives a reference for the absolute intensity of temperature fluctuations, while the locally normalized result θ_c'/Θ_c provides a ratio which has been found by previous researchers to asymptote to a constant in the self-similar far-field region. Figure 17 shows that the exit conditions influence the development of $\theta_c'(x)$ throughout the flow. For the smooth contraction, the near-field growth rate of θ_c' is significantly higher than for the pipe case. The maximum absolute value of θ_c' for the smooth contraction nozzle ($= 0.135\Theta_e$) is 145% higher than that for the pipe ($= 0.055\Theta_c$). The axial location of the maximum of θ_c'/Θ_e is found at $x \approx 5d$ for the smooth contraction, compared to $x \approx 8d$ for the pipe. In each case, this location of maximum of the ratio θ_c'/Θ_e is slightly downstream from the end of the average potential core (Mi, Nathan & Luxton 2000).

It can be argued that the above difference in θ_c' is a direct consequence of the difference in the near-field flow structure of the two jets. For the jet from the smooth contraction, strong large-scale engulfment of ambient 'cold' air by the highly coherent vortex structures, present in the near field (figure 10*a*), results in a high amplitude of the temperature fluctuations and, thus, a rapid growth of θ_c'. By contrast, for the pipe case, the lack of the large-scale coherent structures (see figure 10*b*) leads to a relatively weak engulfment of surrounding 'cold' air into the jet in the near-field region; as a result, the amplitude of the temperature fluctuations in the jet core region is lower.

We now consider the centreline evolution of the locally normalized r.m.s. $\theta_c^* \equiv \theta_c'/\Theta_c$. As reported in § 2, previous studies suggest that the evolution of θ_c^* in the jets from the smooth contraction nozzles (figure 4*a*) differs markedly from that in the pipe jets (figure 4*b*). This difference is more clearly illustrated in figure 17. For the smooth contraction case, θ_c^* has a distinct hump immediately downstream from the potential

core of the jet. The height of the hump is expected to reflect the strength of the overall interaction between coherent vortical structures and the induced (unmixed or partially mixed) ambient fluid. For the pipe case, no hump exists in θ_c^* even around $x/d \approx 8$ at which θ_c' is maximum; θ_c^* grows asymptotically towards a constant value in the self-similar far field.

The self-similar nature of the fluctuating scalar field of the two jets can be interpreted from the far-field measurements of θ_c^*. The asymptotic value $\theta_c^* = \theta_{asy}^*$ for the pipe is lower than that for the smooth contraction. For the smooth contraction case, θ_{asy}^* is approximately 0.236 (averaged over the range $x/d \geqslant 40$), a value which agrees well with that (≈ 0.237) of Dowling & Dimotakis (1990) also obtained in a jet issuing from a smooth contraction nozzle at the same Reynolds number (see table 1). However, for the pipe case, $\theta_{asy}^* = 0.218$ (averaged over the range $x/d \geqslant 50$) is approximately 8% lower than that for the contraction. This difference is too large to be explained by experimental error which has a maximum possible value of $\pm 3\%$ for θ_c^* (estimated from the possible maximum uncertainties of $\pm 1.5\%$ and $\pm 2.0\%$ for the mean Θ_c and the r.m.s. θ_c'), indicating a genuine difference in the flows due to the different exit conditions. The use of identical facilities and measurement technique for all the temperature measurements ensures that the uncertainty in the comparison of one experiment to another is small and should not contribute significantly to the difference observed in figure 17.

6.3. *Probability density function of scalar fluctuations*

Figures 18(*a*) and 18(*b*) show the streamwise evolution of the local, one-point probability density function (p.d.f.) of the passive temperature $\tilde{\Theta}(= \Theta + \theta)$ along the centreline of each jet. Here, the p.d.f., $p(\tilde{\Theta})$, is defined by

$$\overline{\tilde{\Theta}^n} = \int_o^\infty \tilde{\Theta}^n p(\tilde{\Theta})\,\mathrm{d}\tilde{\Theta} \quad \text{and} \quad \int_0^\infty p(\tilde{\Theta})\,\mathrm{d}\tilde{\Theta} = 1, \tag{10}$$

where the integer $n \geqslant 1$. We present the data using the form $p(\Theta^*)$ vs. $\Theta^* = \tilde{\Theta}_c/\Theta_e$. There is a distinct difference between the evolutions of the centreline p.d.f. in the two for $x/d < 20$. It is evident from the figures that $\tilde{\Theta}_c$ in the jet from the contraction exhibits a wider range of variations than does that from the pipe, especially over the region $x/d \leqslant 8$. This fact is highlighted in figure 19 which presents the centreline p.d.f.s of both jets obtained at $x/d = 5$ and 8. To facilitate comparison of the extreme values of $\tilde{\Theta}_c$ which have a low probability, the p.d.f.s are presented in the logarithmic form, i.e. $\log\ p(\Theta^*)$ vs. Θ^*. The locations $x/d = 5$ and 8 are chosen as they correspond to the locations of the maximum of θ_c'/Θ_c associated with the end of the potential core for the smooth contraction and pipe jet flows, respectively. At $x/d = 5$, $\tilde{\Theta}_c$ varies between $0.68\Theta_e$ and $0.98\Theta_e$ in the pipe jet and between $0.2\Theta_e$ and $0.99\Theta_e$ in the contraction jet. As the flows develop to $x/d = 8$, the range of fluctuation of $\tilde{\Theta}_c$ becomes $0.4\Theta_c$–$0.9\Theta_e$ (pipe) and $0.18\Theta_c$–$0.9\Theta_e$ (contraction). For the contraction case, the dominance of the large-scale vortex structures in the near field results in the incursion of 'cold' ambient fluid deep into the core of the jet, even though the 'hot' original jet fluid remains dominant and thus has a higher probability. In contrast, the predominance of smaller-scale structures immediately downstream from the pipe exit results in weaker engulfment of the ambient 'cold' air, leading to a narrower range of temperature fluctuations. With different flow structures, the shape of $p(\Theta^*)$ is quite different for the two jets. The presence of large-scale structures for the contraction case results in the exponential tails that are not present for the pipe case. Note that the shape of the scalar p.d.f. reflects the degree of the small-scale mixing (see Mi *et al.* 1998).

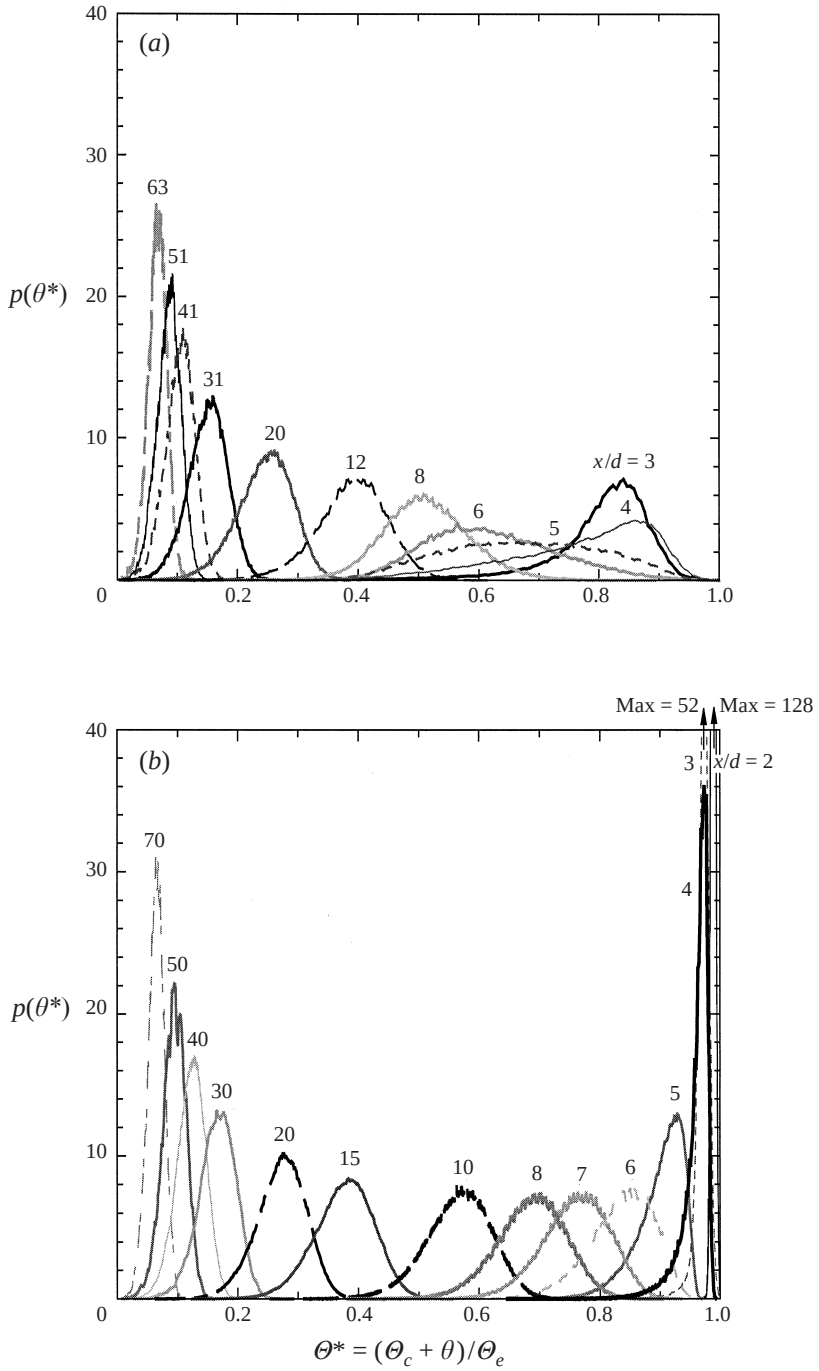

FIGURE 18. Streamwise evolution of the probability density function (p.d.f.), $p(\tilde{\Theta})$, of the temperature $\tilde{\Theta}$: (*a*) smooth contraction; (*b*) pipe.

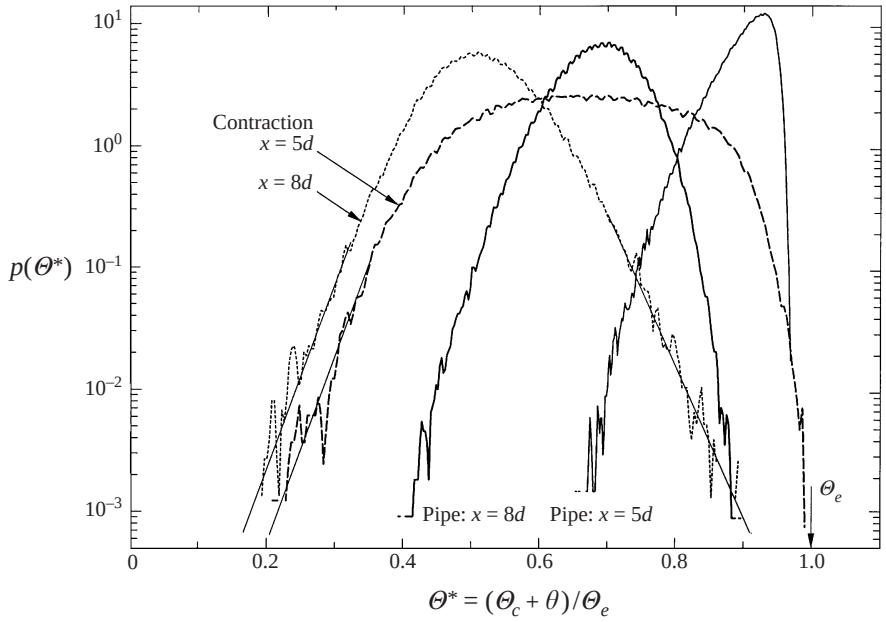

FIGURE 19. The probability density functions, $p(\tilde{\Theta})$, of the temperature $\tilde{\Theta}$ obtained at $x/d = 5$ and 8 in the two jets.

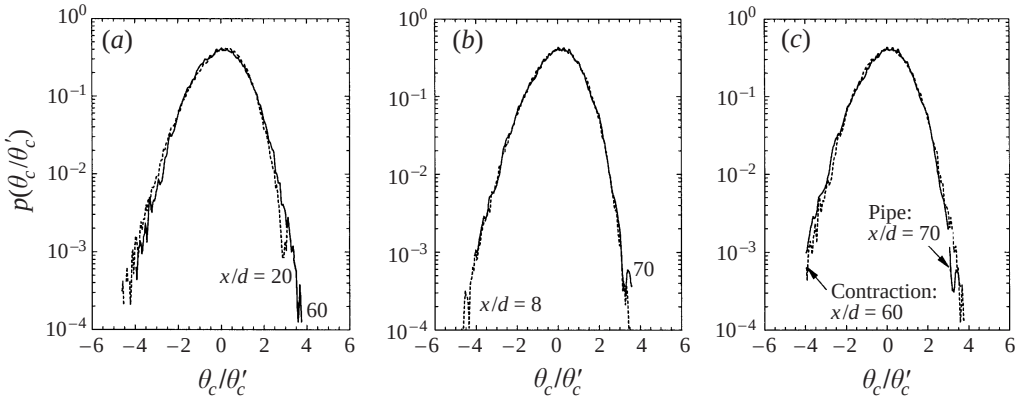

FIGURE 20. The probability density functions $p(\theta)$ of the temperature fluctuations θ obtained (*a*) at $x/d = 20$ and 60 for the contraction case and (*b*) at $x/d = 8$ and 70 for the pipe case. A direct comparison of the two jets is presented in (*c*).

Figure 20 presents the centreline scalar p.d.f.s against the scalar fluctuation normalized by its own r.m.s. (instead of the local mean), i.e. θ_c/θ'_c. This presentation of the p.d.f.s is commonly adopted in the literature. It is perhaps surprising at first glance that, for the pipe jet, $p(\theta_c/\theta'_c)$ appears to have approached the 'asymptotic' shape by only $x/d = 8$, since $p(\theta_c/\theta'_c)$ collapses well for both $x/d \approx 8$ and $x/d \approx 50$. However, the normalized distribution of the p.d.f. against θ_c/Θ_c (not presented here) approaches its asymptotic shape at the same value of x/d as for the self-similarity of θ'_c/Θ_c. In contrast, for the smooth contraction nozzle, the shapes of the p.d.f.s at $x/d = 20$ and 60 still show differences, consistent with the flow not being fully developed at $x/d = 20$. A direct comparison in the shape of the far-field p.d.f. for the

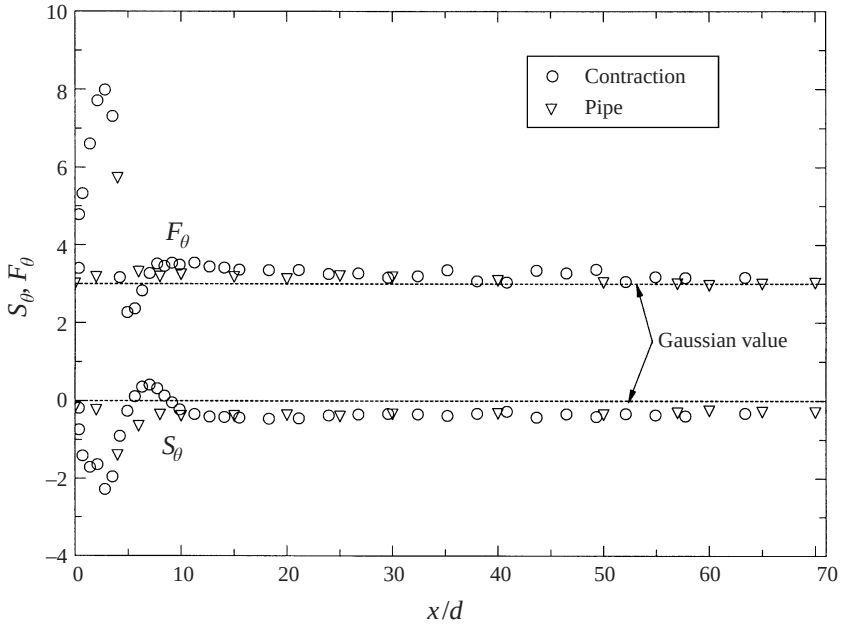

FIGURE 21. Streamwise variation of the skewness (S_θ) and flatness (F_θ) factors of temperature fluctuations θ along the jet centreline.

two jets is presented in figure 20(*c*). A slight difference is revealed, suggesting that differences in the near-field structure propagate into the far field.

The difference in the centreline development of the p.d.f. is reflected in the streamwise evolutions of the skewness $S_\theta \equiv \overline{\theta^3}/\overline{\theta^2}^{3/2}$ and flatness $F_\theta \equiv \overline{\theta^4}/\overline{\theta^2}^2$. Figure 21 shows the axial variations of both S_θ and F_θ along the centreline. Note that S_θ and F_θ were calculated from approximately 200 000 data points of $\theta(t)$ at each x location, so that the convergence of the calculations is satisfactory. Consistent with the p.d.f. data, in the near-field region ($x/d < 20$), these factors behave quite differently for the two jets. However, in contrast with the classical hypothesis of universal similarity, slight difference are found in the far-field asymptotic values of both factors of the two jets, with $(-0.36, 3.20)$ for the contraction case and $(-0.28, 3.07)$ for the pipe case. This difference, albeit small, is still statistically significant because the values of S_θ and F_θ have been averaged over the entire range $x/d \geqslant 25$.

Figures 22 and 23 present the radial distributions of S_θ and F_θ against $\eta = r/(x - x_{o2})$ for the pipe and contraction cases, respectively. The data were obtained at several streamwise locations as indicated on the plots. From the data obtained for the pipe jet, figure 22, self-similarity in the profiles of S_θ and F_θ is achieved much closer to the nozzle exit (by $x/d \approx 20$) than the self-similarity of the r.m.s. fluctuation which does not occur until $x/d \approx 50$ (see figures 16*b* and 17). This, however, is not a contradictory result since S_θ and F_θ are the statistical properties of the fluctuation θ normalized by the r.m.s. value θ' so that they are expected to establish their individual self-similar state relatively early. In contrast, such a disparity does not apply to the jet from the contraction, see figure 23. It is possible that this, and the greater scatter in the data for the contraction nozzle jet, is due to the presence of more large-scale coherent structures in this flow, relative to the pipe jet. The asymptotic radial distributions of S_θ and F_θ are seen to spread over a wider range of η in the jet

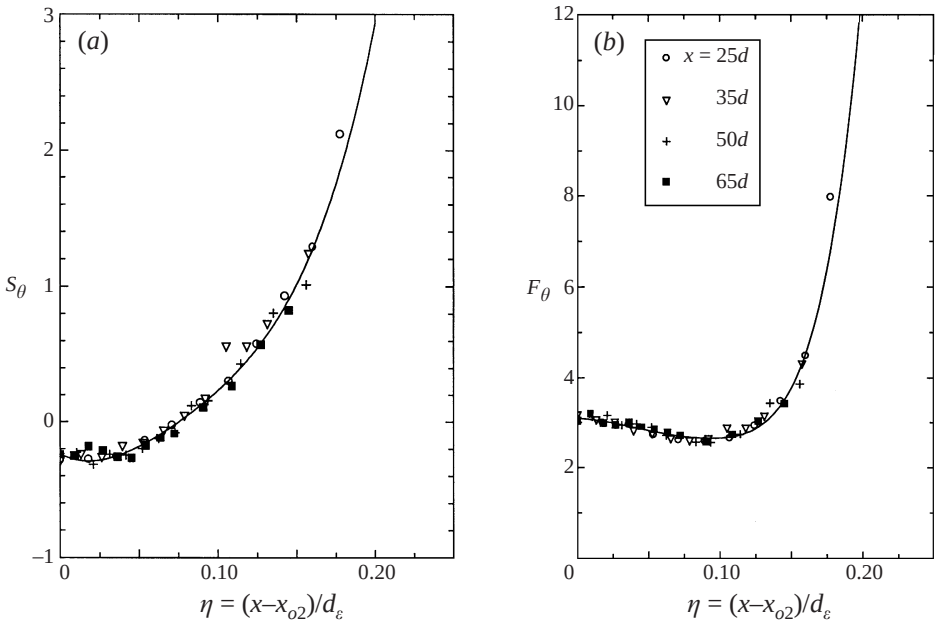

FIGURE 22. Radial distributions of (*a*) the skewness S_θ and (*b*) flatness F_θ against $\eta = r/(x - x_{o2})$, obtained at several streamwise locations as indicated on the plots, for the pipe case.

from the smooth contraction than in the pipe jet. This implies that the p.d.f.s for the two jets are not shaped identically at the same value of η. In other words, the p.d.f. of the passive scalar is *specifically*, but not *generally*, self-similar along rays emanating from the virtual origin of the jet in the far field. This conclusion has also been reached by Dowling & Dimotakis (1990) from an investigation of the axisymmetric jet from a single smooth contraction nozzle and under different Reynolds numbers (Re_d).

7. Further discussion

In the preceding sections, we have reported the statistical properties of the passive scalar field of jets issuing from both a smooth contraction nozzle and a pipe. Not only have differences been identified in the near field but also non-identical states of self-similarity of the turbulent scalar field have been observed. In § 6, the near-field differences have been linked to the significant difference of the turbulence structures shown in § 5. Here, we propose to relate the far-field differences in scalar statistical properties to the underlying turbulence structure in the two jets with different initial conditions. This is followed by a general discussion.

The existence of large-scale coherent structures in the far field of an axisymmetric jet has been demonstrated in previous studies by Sreenivasan (1984), Komori & Ueda (1985), Shlien (1987), Dahm & Dimotakis (1987), Tso & Hussain (1989), Mungal & O'Neil (1989) and Yoda, Hesselink & Mungal (1992). It is important to note however that smooth contraction nozzles were used in all these studies (the nozzle type for Yoda *et al.* was deduced as it was not explicitly stated). Tso & Hussain (1989) observed that the far-field coherent structures are dominated by the helical mode. They used a radial linear rake of X-wire probes to measure the azimuthal vorticity in the diametral plane and conditionally averaged the data to extract the dynamics of the far-field coherent structures. Later, the study of Yoda *et al.* (1992),

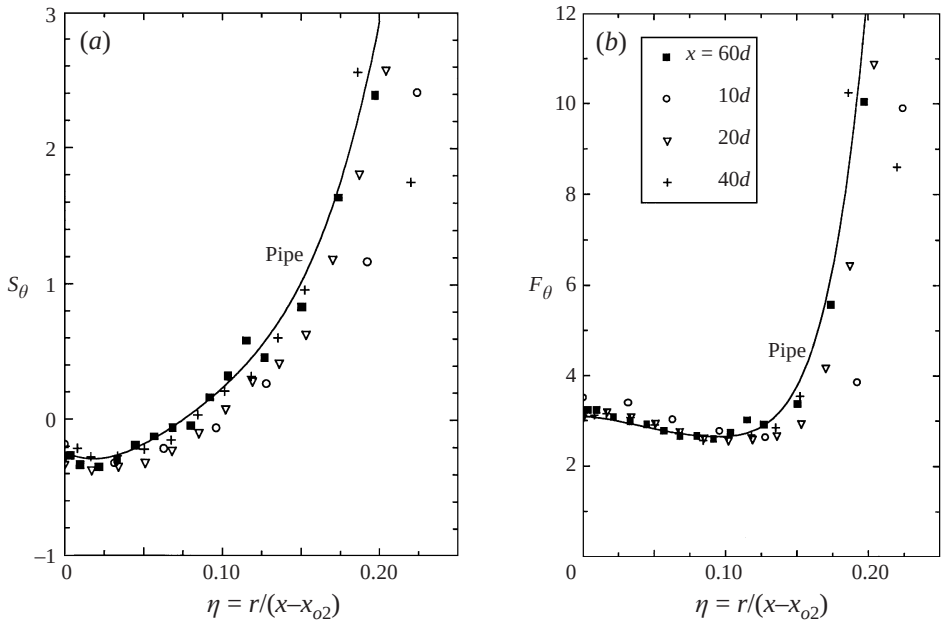

FIGURE 23. Radial distributions of (*a*) the skewness S_θ and (*b*) flatness F_θ against $\eta = r/(x - x_{o2})$, obtained at several streamwise locations indicated on the plot, for the contraction case.

using a planar laser-induced fluorescence (PLIF) technique, suggested that both the helical and axisymmetric modes are important in the far field and that the structure tends to switch between these two modes. They found that the coherent structure is present almost all the time in the far field. This finding was also claimed by Dahm & Dimotakis (1987) and Mungal & O'Neil (1989). Accordingly, it is reasonable to conclude that large-scale coherent structures are always present in the far field of the jet from a smooth contraction nozzle.

Unfortunately, there is less relevant data available on a jet issuing from a long pipe. Our literature survey has only found one relevant study, that carried out by Schefer *et al.* (1994) in the developing region of a methane jet. These authors observed coherent structures and claimed to identify both the axisymmetric and helical modes, stating that the latter mode is less frequent. We note that their detection criteria were qualitative (visual) and that the instantaneous concentration field of view was limited to the axial range $9.6 \leqslant x/d \leqslant 16.6$ (their figures 3–5). It is thus unclear whether their observation can be extended to the far field. As such, no firm conclusion can be made about the nature of the coherent structure in the self-similar region of a jet from a long pipe.

At this stage, we tentatively hypothesize that the coherent structure may only occur intermittently (i.e. not all the time) in the far field of a pipe jet, while it is always present in a jet from a smooth contraction nozzle. This hypothesis can explain the differences between the two jets indicated in figures 14–17. The instantaneous radial profiles of 'top-hat' type or 'two-level' type concentration profiles across the jet from a smooth contraction reported by Dahm & Dimotakis (1987) suggest that the concentration within the large-scale structures is quasi-uniform. In the far field of the jet from the present contraction nozzle, more large-scale coherent structures cause stronger engulfment of the 'cold' ambient fluid. As a result, a wider spread and larger amplitude in fluctuation of the fluid temperature are expected for the

jet from the contraction nozzle than for the pipe case. This is consistent with the larger streamwise variation of the half-radius (figure 15) and the higher value of the normalized centreline r.m.s. temperature fluctuation (figure 17) in the jet issuing from the smooth contraction than those for the pipe jet.

The present experimental results reported above do not support the classical hypothesis that the asymptotic state or self-similarity of a turbulent flow is independent of its initial conditions (e.g. Townsend 1976). This is not exclusive to jet flows. Numerous studies on turbulent wake flows also do not support the hypothesis. For example, Bevilaqua & Lykoudis (1978) compared the wake of a sphere with that of a porous disk, which had the same drag and Reynolds number, and found that the turbulence intensity (normalized by the maximum velocity defect) in the self-similar region is significantly larger in the wake of the sphere than in that of the disk. Later, Wygnanski, Champagne & Marasli (1986) investigated the turbulent planar wakes behind various wake generators, most with identical drag coefficients (thus allowing comparison at identical Reynolds numbers). It was shown that, while the lateral profiles of the normalized streamwise mean velocity are virtually identical for all the far wakes, the lateral profiles of the normalized streamwise turbulence intensity and Reynolds shear stress are quite different even though each wake flow attains self-similarity. Other researchers (Bonnet, Delville & Garem 1986; Louchez, Kawall & Keffer 1987; Zhou & Antonia 1995; Antonia & Mi 1998) subsequently confirmed that the statistical behaviours of a planar, far-wake turbulent flow in the self-similar region varied significantly depending on the initial conditions. Of interest also, in grid turbulence, a simple quasi-homogeneous flow, the effect of initial anisotropy was experimentally found to persist into the final stage of decay of the turbulence (e.g. Batchelor 1953).

8. Conclusions

The present study has explored the influence of jet exit conditions on the passive scalar field of an axisymmetric free jet through an experimental study and a review of the literature. The present experiments were conducted at a Reynolds number of 16 000 using both quantitative point measurements of a passive temperature and velocity and a qualitative planar Mie scattering flow-visualization technique. To generate significantly different exit velocity profiles, a smooth contraction nozzle which produces a 'top-hat' velocity profile and a long straight pipe which produces a jet emerging with fully developed pipe turbulence were used. Previous studies using smooth contraction nozzles and long pipes have also been reviewed.

The present study has revealed that the turbulent scalar properties throughout the jet flow field do depend upon initial conditions. The differences observed in the scalar field of the two jets can be related to differences in the underlying turbulence structure, even in the self-similar region. The present work thus supports the analytical result of George (1989) that the entire flow is influenced by the initial conditions and thus that a variety of self-similar states in the far field are possible due to different initial conditions.

More specifically, the present work has shown that:

(i) The near-field structures in the jets from the two nozzles are quite different. In the flow from the smooth contraction nozzle, well-defined vortical structures are observed which exhibit the roll-up, pairing and break-up process, due to the natural shear-layer instability associated with the initially thin boundary layer and uniform potential core. By contrast, such large-scale coherent structures are not found in the pipe jet because of the thick exit boundary layer, initial turbulent state and non-

uniform velocity in the 'potential core'. Associated with such differences in the flow structure of the two jets is a dramatic difference in the scalar field around the end of the potential core. A strong hump in the normalized r.m.s scalar fluctuations along the centreline occurs immediately downstream from the end of the potential core for the smooth contraction, while no hump is found in the pipe jet (figure 17).

(ii) The asymptotic centreline decay rate of the mean scalar field of the jet issuing from a smooth contraction is a function of Reynolds number (Ebrahimi & Kleine 1977; Dowling & Dimotakis 1990), while that from a long pipe appears to have no Reynolds-number dependence (Pitts 1991*b*; Pitts & Kashiwagi 1984; Richards & Pitts 1993).

(iii) The centreline decay rate of the mean scalar field is larger for the jet issuing from a smooth contraction than that from a long pipe in both the near and far fields.

(iv) In the jet from a smooth contraction nozzle, the asymptotic spreading rate of the scalar field is larger than that for the pipe jet.

(v) The concept of a single virtual origin for a jet, as stated explicitly in the classical similarity treatments of Hinze (1975) and Chen & Rodi (1980), is not supported by the present and many previous investigations (e.g. Richards & Pitts 1993). The virtual origin associated with the streamwise variation of the half-radius is usually different from that for the centreline decay rate of the mean scalar.

(vi) The asymptotic value of the locally normalized r.m.s. of the centreline scalar fluctuations for the jet issuing from a smooth contraction is higher than that for the pipe jet.

(vii) The present radial profiles of the temperature skewness and flatness factors support the finding of Dowling & Dimotakis (1990) that the p.d.f. of the passive scalar is specifically, but not generally, self-similar along rays emanating from the virtual origin.

Both our literature review and experimental investigation of axisymmetric jet flows support the deduction of George (1989), as do previous investigations of wake flows by the researchers cited above. The present findings, taken together with those for other classes of free shear flows discussed in the text, suggest that a universal asymptotic state of turbulence is unlikely to exist for any class of turbulent flow and that turbulence, even in a fully developed state, does not 'forget' its origins. That is, the classical hypothesis of universal similarity, which requires asymptotic independence of initial conditions, is flawed and should not be applied.

The authors gratefully acknowledge the support of the Australian Research Council through the Large and SPIRT Grant schemes. The work has been conducted within the Turbulence, Energy & Combustion Research Group, University of Adelaide, with contribution from numerous Group members through various informal discussions. We also appreciate the comments from all three referees, which have strengthened the final draft of this paper.

Appendix. Relation between jet initial momentum addition rate (J_e) and Reynolds number (Re_d)

The jet momentum addition rate J_e can be expressed, based on the mean velocity profile $U_e(r)$ and the fluid density at the round nozzle exit whose diameter is d, as

$$J_e = \int_0^{d/2} 2\pi\rho_e U_e^2 r \, \mathrm{d}r. \tag{A 1}$$

Using $\xi = r/d$, $g(\xi) = U_e(r)/U_e(0)$ and $A = \int_0^{1/2} g^2(\xi)\xi \, \mathrm{d}\xi$, (A1) may be re-written as

$$J_e = 2\pi d^2 \rho_e U_e^2(0) A \tag{A 2}$$

for an incompressible fluid. The Reynolds number based on jet initial conditions is $Re_d = U_o d/\nu$. Here, U_o is the exit bulk velocity and may be calculated from $U_e(r)$ as follows:

$$U_o = \frac{4}{\pi d^2} \int_0^{d/2} 2\pi U_e r \, \mathrm{d}r = 8U_e(0) \int_0^{1/2} g(\xi)\xi \, \mathrm{d}\xi.$$

With $B = \int_0^{1/2} g(\xi)\xi \, \mathrm{d}\xi$, the Reynolds number may be expressed as

$$Re_d = 8B \frac{U_e(0)\, \mathrm{d}}{\nu}. \tag{A 3}$$

From (A2) and (A3), we obtain the ratio

$$\frac{J_e}{Re_d^2} = \frac{\pi}{32} \rho_e \nu^2 \frac{A}{B^2}. \tag{A 4}$$

The relation (A4) indicates that, for different jets emerging from a single type (e.g. smooth contraction or pipe) of nozzle, use of the same value of Re_d means identical initial momentum addition rates. For jets issuing from different types of nozzles, however, this conclusion cannot be obtained directly from (A4). Nevertheless, we can show below that the same value of Re_d corresponds to a nearly identical value of J_e for different axisymmetric jets issuing, respectively, from a long pipe and a smooth contraction nozzle. For the jet from a smooth contraction nozzle, a top-hat velocity profile, i.e. $g \approx 1$, makes $A \approx B \approx 1/8$, so that

$$\frac{J_e}{Re_d^2} \approx 0.25\pi \rho_e \nu^2. \tag{A 5}$$

For the fully developed pipe flow jet, it is well known that the initial velocity profile may be expressed approximately by the empirical power-law profile $g = (1 - 2\xi)^{1/n}$, where $n = 6$–10 depending on Re_d (e.g. Munson *et al.* 1998, pp. 484–485). From this profile, it is obtained that $A = \int_0^{1/2} (1 - 2\xi)^{2/n} \xi \, \mathrm{d}\xi = 0.0803$–$0.0946$ and $B = \int_0^{1/2} (1 - 2\xi)^{1/n} \xi \, \mathrm{d}\xi = 0.0987$–$0.108$ for $n = 6$–10. Hence, for the pipe jet, (A4) becomes

$$\frac{J_e}{Re_d^2} = 0.253\pi \rho_e \nu^2 \sim 0.257\pi \rho_e \nu^2. \tag{A 6}$$

From (A5) and (A6), if $(Re_d)_{\mathrm{pipe}} = (Re_d)_{\mathrm{contr}}$ and the same jet fluid is used, $(J_e)_{\mathrm{pipe}}$ is only slightly greater (1.2–2.8%) than $(J_e)_{\mathrm{contr}}$. In other words, the same Re_d used for the two jets can lead to nearly identical momentum addition rates. This conclusion holds even accounting for the effect of the initial velocity fluctuations on J_e. Note that the initial lateral velocity fluctuations are negligible in both flows. Accordingly, the momentum integral (A1) may be approximated, to second order (e.g. Hussein *et al.* 1994), by

$$J_e = \int_0^{d/2} 2\pi \rho_e U_e^2 (1 + \overline{u^2}/U_e^2) r \, \mathrm{d}r. \tag{A 7}$$

Because of the ratio $\overline{u^2}/U_e^2$ being generally small across the jet nozzle, even for the pipe jet (< 0.05), the effect that the velocity fluctuation has on J_e should be negligible. For example, using the present profile of $\overline{u^2}/U_e^2$, J_e increases only 1% for the pipe jet and 0.2% for the contraction jet, compared with that obtained by (A 1).

REFERENCES

Antonia, R. A. & Bilger, R. W. 1973 An experimental investigation of an axisymmetric jet in a co-flowing air stream. *J. Fluid Mech.* **61**, 805–822.

Antonia, R. A. & Bilger, R. W. 1976 The heated round jet in a co-flowing stream. *AIAA J.* **14**, 1541–1547.

Antonia, R. A. & Mi, J. 1998 Approach towards self-similarity of turbulent cylinder and screen wakes. *Exptl Therm. Fluid Sci.* **17**, 277–284.

Batchelor, G. K. 1953 *Homogeneous Turbulence*. Cambridge University Press.

Becker, H. A., Hottel, H. C. & Williams, G. C. 1967 The nozzle fluid concentration field of the round turbulent jet. *J. Fluid Mech.* **30**, 285–303.

Beer, J. M., Chigier, N. A. & Lee, K. B. 1962 Modelling of double centric burning jets. *9th Symp.* (*Intl*) *on Combustion*, pp. 892–900. The Combustion Institute.

Bevilaqua, P. M. & Lykoudis, P. S. 1978 Turbulence memory in self-preserving wake. *J. Fluid Mech.* **80**, 589–606.

Birch, A. D., Brown, D. R., Dodson, M. D. & Thomas, J. R. 1978 The turbulent concentration field of a methane jet. *J. Fluid Mech.* **88**, 431–449.

Boersma, B. J., Brethouwer, G. & Nieuwstadt, F. T. M. 1998 A numerical investigation on the effect of the inflow conditions on the self-similar region of a round jet. *Phys. Fluids* **10**, 899–909.

Bonnet, J.-P., Delville, J. & Garem, H. 1986 Space and space-time longitudinal velocity correlations in the turbulent far wake of a flat plate in incompressible flow. *Exps. Fluids* **7**, 475-480.

Bradshaw, P. 1966 The effect of initial conditions on the development of a free shear layer. *J. Fluid Mech.* **26**, 225–236.

Brown, G. L. & Roshko, A. 1974 On density effects and large structure in turbulent mixing layers. *J. Fluid Mech.* **64**, 775.

Browne, L. W. B., Antonia, R. A. & Chamber, A. J. 1984 The interaction region of a turbulent plane jet. *J. Fluid Mech.* **149**, 355–373.

Chen, C. J. & Rodi, W. 1980 *Vertical Turbulent Buoyant Jets – A Review of Experimental Data*. Pergamon.

Chua, L. P. & Antonia, R. A. 1986 The turbulent interaction region of a circular jet. *Intl Commun. Heat Mass Transfer* **13**, 545–558.

Crow, S. C. & Champagne, F. H. 1971 Orderly structure in jet turbulence. *J. Fluid Mech.* **48**, 547–591.

Dahm, W. J. A. & Dimotakis, P. E. 1987 Measurements of entrainment and mixing in turbulent jets. *AIAA J.* **25**, 1216–1223.

Dahm, W. J. A. & Dimotakis, P. E. 1990 Mixing at large Schmidt number in the self-similar far field of turbulent jets. *J. Fluid Mech.* **217**, 299–330.

Dowling, D. R. 1988 Mixing in gas phase turbulent jets. PhD thesis, California Institute of Technology, Pasadena CA.

Dowling, D. R. & Dimotakis, P. E. 1990 Similarity of the concentration field of gas-phase turbulent jets. *J. Fluid Mech.* **218**, 109–141.

Dziomba, B. & Fiedler, H. E. 1985 Effect of initial conditions on two-dimensional free shear layers. *J. Fluid Mech.* **152**, 419.

Ebrahimi, I. & Kleine, R. 1977 Konzentrationsfelder in isothermermen Luft-Freistrahlen. *Forsch. Ing.* **43**, 25–30.

Flora, J. J. & Goldschmidt, V. M. 1969 Virtual origins of a free plane turbulent jet. *AIAA J.* **7**, 2344–2346.

George, W. K. 1989 The self-similarity of turbulent flows and its relation to initial conditions and coherent structures. In *Recent Advances in Turbulence* (ed. R. E. A. Arndt & W. K. George), pp. 39–73. Hemisphere.

George, W. K. 1990 Governing equations, experiments and experimentalist. *Exptl Therm. Fluid Sci.* **3**, 557–566.

George, W. K. 1995 Some new ideas for the similarity of turbulent shear flows. *Proc. ICHMT Symp. on Turbulence, Heat and Mass Transfer, Lisbon 1994* (ed. Hanjalic & Peiera), pp. 13–24. Begell House.

Gouldin, F. C., Schefer, R. W., Johnson, S. C. & Kollmann, W. 1986 Nonreacting turbulent mixing flows. *Prog. Energy Combust. Sci.* **12**, 257–303.

Grandmaison, E. W., Rathgeber, D. E. & Becker, H. A. 1982 Some characteristics of concentration fluctuations in free turbulent jets. *Can. J. Chem. Engng* **60**, 212–219.

Grinstein, F. F., Glauser, M. N. & George, W. K. 1995 Vortex in jets. In *Fluid Vortices* (ed. S. I. Green), Chap. III. Kluwer.

Hinze, J. O. 1975 *Turbulence*, 2nd Edn. McGraw-Hill.

Ho, C. W. & Nosseir, N. S. 1981 Dynamics of an impinging jet. Part 1. The feedback phenomenon. *J. Fluid Mech.* **105**, 119–142.

Hussain, F. & Clark, A. R. 1981 On the coherent structure of the axisymmetric mixing layer: a flow-visualization study. *J. Fluid Mech.* **104**, 263–294.

Hussain, F. & Ramjee, V. 1976 Effects of the axisymmetric contraction shape on incompressible turbulent flow. *Trans. ASME: J. Fluids Engng* **98**, 58–69.

Husain, D. Z. & Hussain, F. 1979 Axisymmetric mixing layer: influence of the initial and boundary conditions. *AIAA J.* **17**, 48.

Hussein, H. J., Capp, S. P. & George, W. K. 1994 Velocity measurements in a high Reynolds number, momentum-conserving axisymmetric turbulent jet. *J. Fluid Mech.* **258**, 31–60.

Komori, S. & Ueda, H. 1985 The large-scale coherent structure in the intermittent region of the self-preserving round free jet. *J. Fluid Mech.* **152**, 337–359.

Lockwood, F. C. & Moneib, A. 1980 Fluctuating temperature measurements in a heated round free jet. *Combust. Sci. Tech.* **22**, 63–81.

Louchez, P. R., Kawall, J. G. & Keffer, J. F. 1987 Detailed spread on characteristics of plane wakes. In *Turbulent Shear Flow* 5 (ed. F. Durst, B. E. Launder, J. L. Lumley, F. W. Schmidt & J. H. Whitelaw), pp. 98–109, Springer.

Malmström, T. G., Kirkpatrick, A. T., Christensen, B. & Knappmiller, K. D. 1997 Centreline velocity decay measurements in low-velocity axisymmetric jets. *J. Fluid Mech.* **346**, 363–377.

McQuaid, J. & Wright, W. 1974 Turbulence measurements with hot-wire anemometry in non-homogeneous jets. *Intl J. Heat Mass Transfer* **17**, 341–349.

Mi, J., Antonia, R. A., Nathan, G. J. & Luxton, R. E. 1998 Non-Gaussian statistics of a passive scalar in turbulent flows. *Proc. Combust. Inst.* **27**, 989–996.

Mi, J., Nathan, G. J. & Luxton, R. E. 2000 Centreline mixing characteristics of jets from nine differently shaped nozzles. *Exps. Fluids* **23**, 93–95.

Mungal, M. G. & O'neil, J. M. 1989 Visual observation of turbulent diffusion flames. *Combust. Flames* **78**, 377–389.

Munson, B. R., Young, D. F. & Okiishi, T. H. 1998 *Fundamentals of Fluid Mechanics*, 3rd Edn, pp. 483–488. John Wiley.

Nickels, T. B. & Perry, A. E. 1996 An experimental and theoretical study of the turbulent coflowing jet. *J. Fluid Mech.* **309**, 157–182.

Nobes, D. 1997 The generation of large-scale structures by jet precession. PhD thesis, Department of Mechanical Engineering, University of Adelaide, Australia.

Papadopoulos, G. & Pitts, W. M. 1998 Scaling the near-field centerline mixing behavior of axisymmetric turbulent jets. *AIAA J.* **36**, 1635–1642.

Pitts, W. M. 1991*a* Effects of global density ratio on the centerline mixing behavior of axisymmetric turbulent jets. *Exps. Fluids* **11**, 125–134.

Pitts, W. M. 1991*b* Reynolds number effects on the centerline mixing behavior of axisymmetric turbulent jets. *Exps. Fluids* **11**, 135–144.

Pitts, W. M. & Kashiwagi, T. 1984 The application of laser-induced Rayleigh light scattering to the study of turbulent mixing. *J. Fluid Mech.* **141**, 391–429.

Richards, C. D. & Pitts, W. M. 1993 Global density effects on the self-preservation behaviour of turbulent free jets. *J. Fluid Mech.* **245**, 417–435.

Russ, S. & Strykowski, P. J. 1993 Turbulent structure and entrainment in heated jets: The effect of initial conditions. *Phys. Fluids* A **5**, 3216–3225.

Schefer, R. W., Kerstein, A. R., Namazian, M. & Kelly, J. 1994 Role of large-scale structure in a nonreacting turbulent CH_4 jet. *Phys. Fluids* **6**, 652–661.

Schlichting, H. 1968 *Boundary Layer Theory*, Chap. 7. McGraw-Hill.

Shlien, D. J. 1987 Observation of dispersion of entrained fluid in the self-preserving region of a turbulent jet. *J. Fluid Mech.* **183**, 163–173.

Smith, D. J. & Hughes, T. 1977 Some measurements in a turbulent circular jet in the presence of a co-flowing free stream. *Aero. Q.* **XXVIII**, 185–196.

So, R. M. C., Zhu, J. Y., Ötügen, M. V. & Hwang, B. C. 1990 Some measurements in a binary gas jet. *Exps. Fluids* **9**, 273–284.

Sreenivasan, K. R. 1984 The azimuthal correlations of velocity and temperature fluctuations in an axisymmetric jet. *Phys. Fluids* **27**, 867–875.

Sreenivasan, K. R. 1996 The passive scalar spectrum and the Obukhov–Corrsin constant. *Phys. Fluids* **8**, 189–196.

Tennekes, H. & Lumley, J. L. 1972 *A First Course in Turbulence*. MIT Press.

Thring, M. W. & Newby, M. P. 1953 Combustion length of enclosed turbulent flames. *Fourth* (*Intl*) *Symp. Combust*., pp. 789–796. The Williams & Wilkins Co.

Townsend, A. A. 1976 *The Structure of Turbulent Shear Flow*, 2nd edn. Cambridge University Press.

Tso, J. & Hussain, F. 1989 Organized motions in a fully developed turbulent axisymmetric jet. *J. Fluid Mech.* **203**, 425–448.

Winant, C. D. & Browand, F. K. 1974 Vortex pairing: The mechanism of turbulent mixing-layer growth at moderate Reynolds number. *J. Fluid Mech.* **63**, 237–255.

Wygnanski, I., Champagne, F. & Marasli, B. 1986 On the large-scale structures in two dimensional, small-deficit, turbulent wakes. *J. Fluid Mech.* **168**, 31–71.

Yoda, M., Hesselink, L. & Mungal, M. G. 1992 The evolution and nature of large-scale structures in the turbulent jet. *Phys. Fluids* A **4**, 803–811.

Yule, A. J. 1978 Large-scale structure in the mixing layer of a round jet. *J. Fluid Mech.* **89**, 412–432.

Zaman, K. B. M. Q. & Hussain, A. K. M. F. 1984 Natural large-scale structures in the axisymmetric mixing layer. *J. Fluid Mech.* **138**, 325–351.

Zhou, Y. & Antonia, R. A. 1945 Memory effects in a turbulent plane wake. *Exps. Fluids* **19**, 112–120.